1 Introduction

The solution of the inverse scattering problem requires, in essence, an inversion of a nonlinear mapping. There are two major difficulties associated with this nonlinear problem in two and three dimensions: ill-posedness and local minima, neither of which has been addressed satisfactorily. The fact alone that the nonlinear mapping at high wave number is extremely oscillatory and therefore possesses numerous local minima renders the most popular approach—nonlinear optimization and its various modifications—fundamentally unreliable. In another notable approach to attacking the nonlinear problem, the original boundary value problem is reformulated as an initial value problem. The resulting method (widely known as layer-stripping) avoids the problem of local minima, only to be plagued by ill-posedness. It seems that there is no inversion method able to solve one problem without being undermined by the other.

In this paper, we present a stable method that solves the inverse scattering problem. The new approach is based on the observation that ill-posedness of the inverse problem can be benefically used to solve it. It measn that not all equations of the nonlinear problem are strongly nonlinear due to the ill-posedness, and that when solved recursively in a proper order, they can be reduced to a collection of essentially linear problems. The algorithm requires multi-frequency scattering data, and the recursive linearization is achieved by a standard perturbational analysis on the wave number k. At each frequency k, the algorithm determines a forward model which produces the presribed scattering data. It first solves nearly linear equations at the lowest k to obtain low-frequency modes of the true scatterer. The approximation is then used to linearize equations at the next higher k to produce a better approximation which contains more modes of the true scatterer, and so on, till a sufficiently high wave number k where the dominant modes of the scatterer are essentially recovered. The underlying physics which permits the gradual recovery is the so-called uncertainty principle: it is increasingly difficult to determine features of the scatterer as their sizes become decreasingly smaller than a half of a wavelength.

The plan of the paper is as follows: in Section 2, we summerize the relevant analytical apparatus, in Section 3 we reformulate the ill-posedness and the inverse scattering problem, and present the inversion method, and in Section 4 we describe the numerical implementation of the algorithm. The robustness of the procedure is demonstrated in Section 5 with numerical examples of inversion of the Helmholtz equation in two dimentsions.

Remark 1.1 *Although our numerical experiments demonstrate convergence and stability of the inversion algorithm, its analysis is presently incomplete. Therefore, the results presented in this paper should be viewed as experimental.*

2 The Mathematical Preliminaries

In this section we introduce the scattering matrix, reformulate the scattering problem as an initial value problem of the Riccati matrix equation for the scattering matrix, and present several basic properties of the scattering matrix.

2.1 The Scattering Problem

The subject of this paper is the inverse scattering problem for Helmholtz equation in two dimensions

$$\Delta\phi(x,y) + k^2(1+q(x,y))\phi(x,y) = 0. \tag{1}$$

In (1), k is a real number, q a smooth function, with $q(x) > -1$ for all $x \in \mathbb{R}^2$. We will be referring to k as the wave number or frequency, to the function q as the scatterer or the forward model. We assume that the support of q is the disk $D(\varpi)$ for some $\varpi > 0$. We will be considering solutions of equation (1) of the form $\phi(x,y) = \phi_0(x,y) + \psi(x,y)$ where $\phi_0 : D(\varpi) \to C$ is a radiation field in $D(\varpi)$, and $\psi : \mathbb{R}^2 \to C$ is a radiation field outside $D(\varpi)$. We will be referring to ϕ as the total field, to ϕ_0 as the incident field, and to ψ as the scattered field. Furthermore, given an incident field ϕ_0 we will be referring to the determination of the corresponding scattered field as the (forward) scattering problem.

Remark 2.1 *We measure the size of the scatterer by the number of wavelengths through the longest ray tube. More precisely, suppose that the curve $\ell \subset D(\varpi)$ is the longest ray tube; then the number of wavelengths across ℓ is given by the formula is*

$$N_w = \frac{k}{2\pi}\int_\ell \sqrt{1+q(x,y)}d\ell. \tag{2}$$

When the medium is quite homogeneous, namely, when q is small, and thus the ray path is roughly straight, (2) is reduced to $N_w = k\cdot\varpi/\pi$.

2.2 The Scattering Matrix and Scattering Data

In this subsection, we reformulate the scattering problem via the scattering matrix; see Section A.1 for the use of notation here. For a more complete description and analysis of the scattering matrix, see [11]. It follows from the well-posedness of the scattering problem and Lemma A.2 that the sequence $\{\alpha_j\} \in Y_{k\varpi}$ of an incident field (96) upon the scatterer q in $D(\varpi)$ uniquely and linearly determines the sequence $\{\beta_j\} \in X_{k\varpi}$ of the scattered field (97). Therefore, there is a linear mapping $S_{\varpi,k} : X_{k\varpi} \mapsto Y_{k\varpi}$ such that $\beta = S_{\varpi,k}\cdot\alpha$; it is refered to as the scattering matrix corresponding to the scatterer q in $D(\varpi)$. For a fixed $k > 0$, the scattering matrix is evidently all we can acquire from scattering measurements outside the disk $D(\varpi)$. The set of matrices

$$\{\, S_{\varpi,k} \mid 0 < k < \infty \,\} \tag{3}$$

is all the information we can collect from real-frequency measurements, and is defined as our scattering data.

Remark 2.2 *The knowledge of the scattering matrix $S_{\varpi,k}$ is equivalent to that of the full-aperture measurements taken outside $D(\varpi)$: the acquisition of each scattered field ψ outside $D(\varpi)$ corresponding to every possible incident field ϕ_0.*

2.3 The Riccati Matrix Equation

For a more complete discussion of the Riccati matrix equation for the scattering matrices, see [11]. For $r > 0$, following the standard procedure of invariant imbedding, we define the chopped scatterer $q_{D(r)}$ by the formula

$$q_{D(r)}(\rho,\theta) = \begin{cases} q(\rho,\theta) & \text{if } \rho < r, \\ 0 & \text{if } \rho \geq r. \end{cases} \tag{4}$$

We denote by $S_{r,k} : Y_{kr} \mapsto X_{kr}$ the scattering matrix corresponding to the chopped scatterer so that for all $\alpha \in Y_{kr}$

$$\beta = S_{r,k}\cdot\alpha \in X_{kr}. \tag{5}$$

Obviously, for any $r \geq \varpi$, $S_{r,k} = S_{\varpi,k}$. At $r = 0$, the chopped scatterer $q_{D(r)}$ is identically zero; any incident field generates no scattered field. Thus,

$$S_{0,k} = 0. \tag{6}$$

As a function of r, the scattering matrix $S_{r,k}$ satisfies a Riccati equation (see (89), (90), (100) for use of notation, see also [11] for more details).

Lemma 2.3 *For any $k > 0$ and all $r \geq 0$, the scattering matrix $S_{r,k} : Y_{kr} \mapsto X_{kr}$ is a solution of the Riccati equation*

$$\frac{dS_{r,k}}{dr} = \frac{i\pi r}{2}k^2(J_{kr} + S_{r,k}\cdot H_{kr})\cdot\hat{q}_r\cdot(H_{kr}\cdot S_{r,k} + J_{kr}). \tag{7}$$

Remark 2.4 *It follows from formulae (5), (87), (88) and Remark A.1 that*

$$(S_{r,k})_{m,n} = O\left(H_m^{-1}(kr)\right), \tag{8}$$

$$(S_{r,k})_{n,m} = O\left(J_m(kr)\right), \tag{9}$$

$$(S_{r,k}\cdot H_{kr})_{m,n} = O\left(H_m^{-1}(kr)\right), \tag{10}$$

$$(H_{kr}\cdot S_{r,k})_{n,m} = O\left(J_m(kr)\right) \tag{11}$$

for an arbitrary integer n and large integer $m \geq N_0(kr)$. Thus, (8), (9) imply that an entry of $S_{r,k}$ whose row or column index is greater in absolute value than $N_0(kr)$ is essentially zero (see Figure 1): $S_{r,k}$ is effectually a square matrix of dimension $2\cdot N_0(kr)$. Similarly, the matrix $S_{r,k}\cdot H_{kr}$ has only $2\cdot N_0(kr)$ effectually nonzero rows, whereas $H_{kr}\cdot S_{r,k}$ has only $2\cdot N_0(kr)$ effectually nonzero columns (see Figure 2).

The structures of the first quadrants (entries with both row and column indices positive) of the matrices $S_{r,k}$, $S_{r,k}\cdot H_{kr}$ and $H_{kr}\cdot S_{r,k}$ are depicted in Figures 1 and 2; a part of a matrix is labeled zero to indicate that the entries there are essentially zero.

Remark 2.5 *Given $k > 0$, the forward scattering problem (see Section 2.1) defines a nonlinear mapping from the scatterer q in $D(\varpi)$ to the scattering data $S_{\varpi,k}$. Since there are only $2\cdot N_0(k\varpi))^2$ essentially nonzero entries in $S_{\varpi,k}$, there will be the same number of equations in the nonlinear system.*

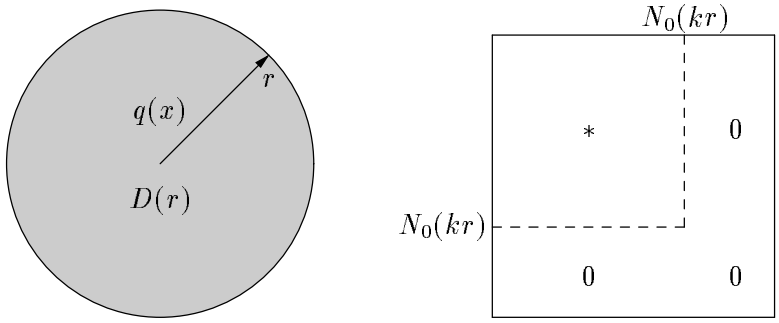

Figure 1: Scatterer on $D(r)$ and Structure of Its Scattering Matrix $S_{r,k}$.

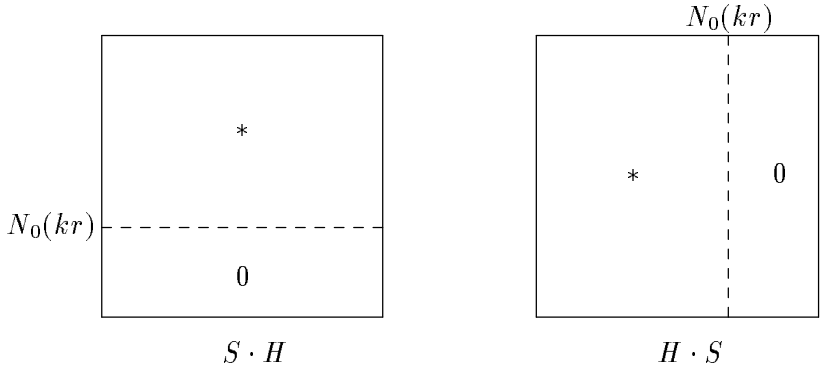

Figure 2: Structures of the Matrices $S_{r,k} \cdot H_{kr}$, $H_{kr} \cdot S_{r,k}$.

2.4 The Far Field

In this subsection, we first define the far field of a scattered field, and link it to the scattering matrix. We then introduce the translation operator of the scattering matrix. For the scattered field ψ, it is well-known (see, e.g., [6]) that the function

$$\psi_\infty(\theta) = \lim_{r \to \infty} \frac{\psi(r, \theta)}{\sqrt{\frac{2}{\pi kr}} e^{i(kr - \pi/4)}} \tag{12}$$

exists and is referred to as the far field of ψ. Given $\beta \in [0, 2\pi]$ and the incident field $\phi_0(x, y) = e^{ik(x\cos\beta + y\sin\beta)} = e^{ikr\cos(\theta-\beta)}$, we denote by $\psi(r, \theta; \beta)$ the corresponding scattered field, and by $\psi_\infty(\theta, \beta)$ its far field. This far field is also known as the full-aperture scattering amplitude (see, for example, [2] and [6]), and is related to the scattering matrix via orthogonal transforms specified in the following lemma which is a reformulation of formula (2.13) of [6] in two dimensions.

Lemma 2.6 *Suppose that b is a positive number and S is the scattering matrix corresponding to a scatterer in the disk $D(b)$. Suppose further that $\psi_\infty(\theta, \beta)$ is the scattering amplitude. Then*

$$\psi_\infty(\theta, \beta) = \sum_{m,l} i^{(l-m)} \cdot S_{m,l} \cdot e^{i(m\theta - l\beta)}, \tag{13}$$

or equivalently, $\psi_\infty(\theta,\beta) = F_\theta^{-1}\cdot\Lambda^{-1}\cdot S\cdot\Lambda\cdot F_\beta$.

The scattering matrix $S_{\varpi,k}$ corresponding to the scatterer q is said to be centered at the origin $(0,0)$ since the expansions (96) and (97) of the incident and scattered fields are around the origin. Now for the same physical scatterer, if we shift the origin to $\xi = (a,b)$, the new scatterer function will be $q^\xi(x,y) = q(x-a, y-b)$. It has a compact support in the disk of radius $A = \varpi + |\xi|$ centered at the new origin. We denote by $S^\xi_{A,k}$ the scattering matrix corresponding to the same scatterer but centered at ξ. The following lemma is a reformulation of Lemmas 3.2, 3.3 of [7].

Lemma 2.7 *Suppose that q is the function of a smooth scatterer with compact support $D(\varpi)$, that $u = (x_1, y_1)$, $v = (x_2, y_2)$ are two points in $\mathbb{R}^2$, and that $A = \varpi + |u|$, $B = \varpi + |v|$. Suppose further that, corresponding to the same scatterer, $S^u_{A,k}$ and $S^v_{B,k}$ are the scattering matrices centered at u and v. Then*

$$S^v_{B,k} = T^{-1}\cdot S^u_{A,k}\cdot T, \tag{14}$$

where $T : \ell^2 \mapsto \ell^2$ is defined by $T = F\cdot\Gamma\cdot F^{-1}$, and $\Gamma : L^2[0,2\pi] \mapsto L^2[0,2\pi]$ is the diagonal linear mapping defined by $(\Gamma\cdot f)(\theta) = e^{ik[(y_2-y_1)\cdot\cos(\theta)-(x_2-x_1)\cdot\sin(\theta)]}\cdot f(\theta)$ for all $f \in L^2[0,2\pi]$

Remark 2.8 *Since Γ and therefore T are orthogonal mappings, two scattering matrices corresponding to the same scatterer but centered differently are connected to each other by orthogonal transforms; therefore, the two scattering matrices contain the same amount of information about the scatterer.*

2.5 The Near Field

Given $r > 0$ and an incident field ϕ_0 upon the chopped scatterer $q_{D(r)}$, the scattered field ψ is smooth inside $D(r)$, continuous across the circle $|x| = r$, and is the expansion (97) outside $D(r)$, an absolutely convergent series for $\rho > r$. $\psi|_{\rho=r}$ is referred to as the near field. Here, we estimate the rate of convergence of (97) at $\rho = r$.

Lemma 2.9 *Suppose that r is a positive number and that the scatterer q is smooth on $\overline{D(r)}$. Suppose further that $\psi : \mathbb{R}^2 \to C$ is the scattered field corresponding to an incident field $\phi_0 : D(r) \to C$ upon the chopped scatterer $q_{D(r)}$. Then the near field $\psi|_{\rho=r}$ has the expansion $\psi(r,\theta) = \sum_{m=-\infty}^{\infty} b_m\cdot e^{im\theta}$, where there exists $c > 0$ dependent on r, k, q such that $b_m \le c||\phi_0||_2/m^2$ for all $|m| \ge N_0(kr)$.*

Proof. See Section 2.5 in [13] □. If $\phi_0(\rho,\theta) = J_n(k\rho)\cdot e^{in\theta}$ in Lemma 2.9, then it follows from (5) that $b_m = (H_{kr}\cdot S_{r,k})_{m,n}$. We therefore obtain

Lemma 2.10 *Suppose that $r > 0$ and that the scatterer q is smooth on $\overline{D(r)}$. Suppose further that $S_{r,k}$ is the scattering matrix corresponding to the chopped scatterer $q_{D(r)}$. Then there exists $c > 0$ such that*

$$|(H_{kr}\cdot S_{r,k})_{m,n}| \le \frac{c}{m^2}, \tag{15}$$

uniformly for all integers n and m such that $|m| \ge N_0(kr)$.

Remark 2.11 *When m becomes greater in absolute value than kr, the elements on the m-th row of $H_{kr}\cdot S_{r,k}$ begin to decrease; they decay uniformly at the rate $1/m^2$ for $m \geq N_0(kr)$. It follows from Remark 2.4 that $H_{kr}\cdot S_{r,k}$ is essentially a square matrix of dimension $2\cdot N_0(kr)$, see Figure 3. It is easy to show (see [13], Remark 2.27 for details) that $S_{r,k}\cdot H_{kr}$ is also essentially a square matrix of the same dimension.*

Figure 3 shows the structures of the first quadrants of the two matrices $S_{r,k}\cdot H_{kr}$ and $H_{kr}\cdot S_{r,k}$; sections of the matrices are labeled zero to indicate small entries there.

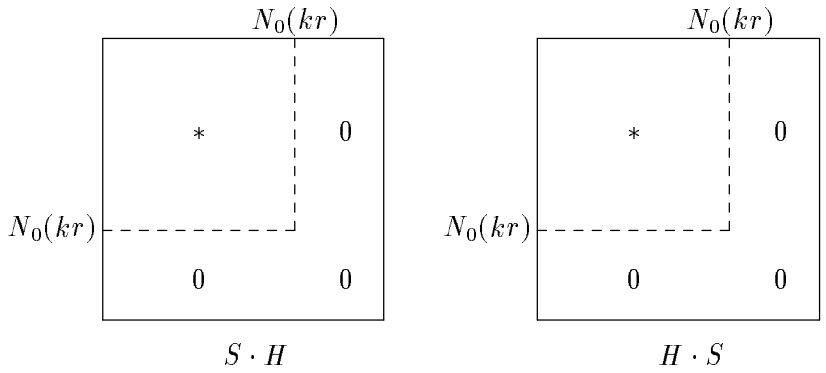

Figure 3: Structures of the Matrices $S_{r,k}\cdot H_{kr}$, $H_{kr}\cdot S_{r,k}$.

3 Heisenberg's Uncertainty Principle and Recursive Linearization

It turns out that the ill-posedness of the inverse scattering problem can be beneficially used to solve it. It means that, due to ill-posedness of the problem, not all equations in the nonlinear system (see Remark 2.5) are strongly nonlinear, and that when solved recursively in a proper order, they can be reduced to a collection of linear problems. In this section, we reformulate the ill-posedness and the inverse scattering problem, and present an inversion algorithm. More specifically, in Section 3.1, we examine and reformulate the ill-posedness of the inverse scattering problem in the special case of weak scattering. In Section 3.2, we briefly and informally describe the recursive linearization method. In Section 3.3, we present the Heisenberg's Uncertainty Principle for the scattering problem, which we shall use in Section 3.4 to reformulate the inverse problem. The details of the inversion algorithm will be described in Section 3.6.

3.1 A Special Case

When q or k is small, the scattered field is weak, and the inverse scattering problem becomes essentially linear. In this subsection, we examine this special case and make necessary connections to the general case where the inverse problem is nonlinear.

Nowhere does the ill-posedness of the inverse scattering problem become more manifest than in the case of weak scattering. As is well-known (see, for example, [8], [12]),

when $k^2 q|\Omega|$ is small (Ω is the support of the scatterer), the scattered field is weak, where the Born Approximation to the far field $\psi_\infty(\theta, \beta)$ (see Section 2.4) can be written in the form

$$\psi_\infty(\theta, \beta) = \frac{ik^2}{4} \int_\Omega q(x, y) e^{ik\{x(\cos\beta - \cos\theta) + y(\sin\beta - \sin\theta)\}} dxdy \tag{16}$$

with an error of $O(q^2)$ when q is small and $k,\ \Omega$ are fixed, or of $O(k^4 \log^2(k))$ when k is small and $q,\ \Omega$ are fixed. In other words, under the assumption of weak scattering, the far field $\psi_\infty(\theta, \beta)$ depends on q essentially linearly, and, up to a higher order error and a scaling, is the Fourier transform of q

$$\hat{q}_{m,n} = \frac{1}{2\pi} \int_\Omega q(x, y) e^{ik(mx+ny)} dxdy \tag{17}$$

with the pair of real numbers m and n given by

$$m = k(\cos\beta - \cos\theta), \tag{18}$$

$$n = k(\sin\beta - \sin\theta). \tag{19}$$

Therefore, the full-aperture far-field measurements

$$\{\ \psi_\infty(\theta, \beta),\ \text{ for all } (\theta, \beta) \in [0, 2\pi] \times [0, 2\pi]\ \} \tag{20}$$

are the Fourier transform $\hat{q}_{m,n}$ for those points (m, n) filling the entire disk $D(2k)$, which we refer to as the Fourier aperture of radius $2k$ (see Figure 5). With such measurements, the scatterer q can be determined, obviously, with the resolution

$$\sigma = \frac{2\pi}{\text{radius of Fourier aperture}} = \frac{2\pi}{2k} = \frac{1}{2}\lambda, \tag{21}$$

where $\lambda = 2\pi/k$ is the wavelength. We consequently have

Lemma 3.1 *(Uncertainty Principle, Small q) Suppose that q is small. Then from the far-field measurements, we cannot determine features of the scatterer that are less than half a wavelength.*

Remark 3.2 *Lemma 3.1 is a reformulation of the ill-posedness of the (linear) inverse problem. It explicitly specifies the null space of the linear operator (16) which maps the scatterer q to the scattering measurements ψ_∞: the Fourier modes of q higher than $2k$ are not observable in the measurements, and thus cannot be determined.*

Remark 3.3 *Formulae (16)—(21) are also valid for small k; therefore, Lemma 3.1 implies that at a sufficiently low frequency only $\hat{q}(0, 0)$ (the average of the scatterer) can be determined from the measurements.*

The scattering matrix $S_{r,k}$ is small if scattering is weak. Thus, for small q or small k, the Riccati equation (7) can be linearized by omitting terms quadratic and cubic in q, $S_{r,k}$ from the equation. The solution of the linearized equation

$$\frac{dS^B_{r,k}}{dr} = \frac{i\pi r}{2} k^2 \cdot J_{kr} \cdot \hat{q}_r \cdot J_{kr} \tag{22}$$

is obviously

$$S^B_{\varpi,k} = \frac{i\pi k^2}{2} \int_0^{\varpi} J_{kr} \cdot \hat{q}_r \cdot J_{kr} \cdot r \cdot dr. \tag{23}$$

Since $S^B_{\varpi,k}$ is an approximation to the scattering matrix $S_{\varpi,k}$, it should be connected to the Born Approximation (16) due to formula (13). The following is a restatement of Lemmas 2.18 of [11] in terms of the scattering matrix.

Lemma 3.4 *Suppose that $S^B_{r,k}$ is the solution of (22), $S_{r,k}$ is the solution of the Riccati equation (7). Then there exists a constant $c > 0$, such that for $k > 0$ and all $r \in [0, \varpi]$,*

$$\|S_{r,k} - S^B_{r,k}\|_2 \leq c \cdot \left(\frac{\frac{5}{2} + |\ln(k\varpi)|}{4} k^2 \cdot \|q\|_\infty \right)^2. \tag{24}$$

Moreover,

$$F_\theta^{-1} \cdot \Lambda^{-1} \cdot S^B_{\varpi,k} \cdot \Lambda \cdot F_\beta = \int_\Omega q(x,y) e^{ik\{x(\cos\beta - \cos\theta) + y(\sin\beta - \sin\theta)\}} dx dy. \tag{25}$$

3.2 The Inversion Algorithm, An Informal Description

Given the wave number $k > 0$, we denote (see Remark 2.5) by

$$P(q,k) = S_{\varpi,k} \tag{26}$$

the system of nonlinear equations for the inverse scattering problem. In this subsection, we briefly describe a simple procedure that solves the inverse problem.

For a given precision $\epsilon > 0$ and frequency $k > 0$, there should be infinite number of forward models q that satisfies (26) to the prescribed precision, due to the ill-posedness of the problem. We choose from them the most smooth one and denote it by q_k. Therefore, to the given precision, the inverse problem can be reformulated as

$$P(q_k,k) = S_{\varpi,k}. \tag{27}$$

We expect that q_k lives in a finite dimensional subspace of L^2, just as it is the case when q is sufficiently small in magnitude where the Fourier transform of q_k is essentially zero outside the disk $D(2k)$ (see Remark 3.2). The inversion algorithm is a recursive linearization procedure which recovers q_k at a number of ascending values of k.

For sufficiently small k, according to Remark 3.3, q_k lives in a one-dimensional subspace; it is the average of q. Moreover, the equation (27) is linear to the prescribed precision ϵ, and therefore can be solved in the least-squares sense to yield q_k.

Now suppose that q_k depends continuously on k, and that we have recovered q_k at some $k > 0$. Then a standard procedure of continuation (see [13], Section 2.6 for details) can be used to recover $q_{k+\delta k}$ by solving a linear problem for the perturbation $\delta q = q_{k+\delta k} - q_k$. Consequently, the inverse scattering problem (26) can be solved up to any given frequency k and to the prescribed precision $\epsilon > 0$, provided that the scattering data (3) are available. In the next several subsections, we characterize more precisely the finite dimensional space where q_k resides, and describe the inversion algorithm in detail.

3.3 Uncertainty Principle, the General Case

According to Lemma 3.4, when q is small and up to the second order of the smallness, the knowledge of the scattering data $S_{\varpi,k}$ is equivalent to the knowledge of the Fourier modes of q in the aperture $D(2k)$. It turns out that when q is not small, the above statement still essentially holds. In other words, $S_{\varpi,k}$ contains information of the Fourier modes of q essentially in $D(2k)$. In this subsection, we wish to make this assertion more precise, and to show it is indeed the case.

In the evaluation of the right hand side of the Riccati equation (7), $J_{kr} + S_{r,k} \cdot H_{kr}$, $H_{kr} \cdot S_{r,k} + J_{kr}$, according to Remarks 2.4 and 2.11, are essentially two square matrices of size $2 \cdot N_0(kr)$. Therefore, the operation

$$(J_{kr} + S_{r,k} \cdot H_{kr}) \cdot \hat{q}_r \cdot (H_{kr} \cdot S_{r,k} + J_{kr}) \tag{28}$$

on $\hat{q}_r$ is a process of low-pass filtering on the scatterer q, as depicted in Figure 4. At a given frequency k and on the circle $|x| = r$, only the Fourier modes

$$\{\ \hat{q}_m(r)\ \mid\ |m| < 2 \cdot N_0(kr)\ \} \tag{29}$$

essentially participate in the operation; higher-frequency modes of the scatterer are filtered out in the process. The relatively low-frequency angular Fourier coefficients (29) at r are therefore picked up in the integration

$$S_{\varpi,k} = \frac{i\pi k^2}{2} \int_0^{\varpi} (J_{kr} + S_{r,k} \cdot H_{kr}) \cdot \hat{q}_r \cdot (H_{kr} \cdot S_{r,k} + J_{kr}) \cdot r \cdot dr, \tag{30}$$

and encoded in the scattering data $S_{\varpi,k}$. We thus conclude that the scattering data contain insignificant information of the higher-frequency angular Fourier coefficients

$$\{\ \hat{q}_m(r)\ \mid\ |m| \geq 2 \cdot N_0(kr)\ \} \tag{31}$$

of the scatterer for all $r \in [0, \varpi]$. In other words, at each $r > 0$, the resolution of the scatterer on the circle $|x| = r$ is

$$\frac{2\pi r}{2N_0(kr)} \approx \frac{\pi}{k} = \frac{1}{2}\lambda. \tag{32}$$

That is, the angular resolution is about half a wavelength. Features of q smaller than half a wavelength in the angular direction contribute considerably weakly to the scattering data; the smaller the features become, the weaker the contributions will be, and the more difficult it becomes to recover these small features. The above discussion is summarized in the following observation.

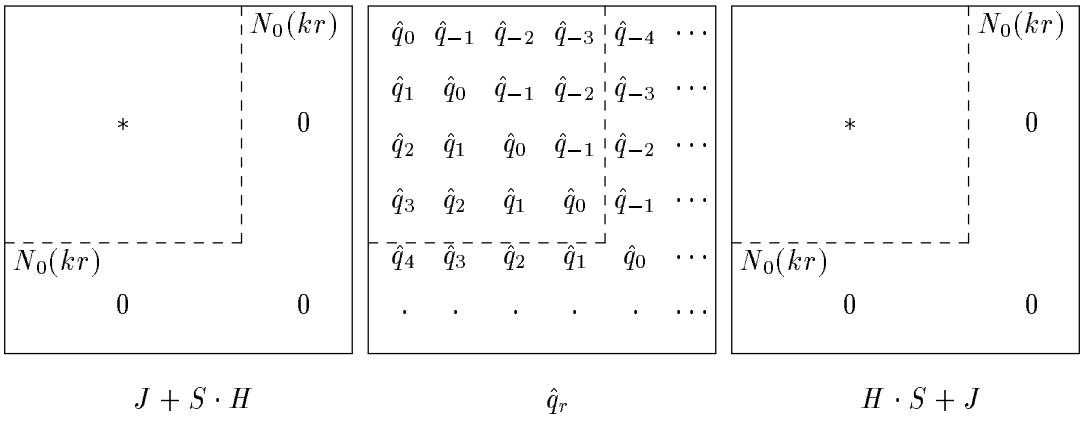

Figure 4: Process of Low-pass Filtering of the Scatterer.

Observation 3.5 *(Uncertainty Principle, Angular Direction) Suppose that the smooth scatterer q has compact support $D(\varpi)$, and that $S_{\varpi,k}$ is the corresponding scattering matrix. Then it is increasingly difficult to determine from $S_{\varpi,k}$ small features of q in the angular direction as their sizes become decreasingly less than half a wavelength.*

We now show that the resolution of the scatterer in an arbitrary direction is also about half a wavelength. Given $\xi = (a, b) \in \mathbb{R}^2$, let $A = \varpi + |\xi|$, and consider the scattering matrix $S^{\xi}_{A,k}$ centered at ξ and corresponding to the scatterer q (see Section 2.4). According to Remark 2.8, $S^{\xi}_{A,k}$ and the scattering data $S_{\varpi,k}$ contain the same amount of information about the scatterer; therefore $S^{\xi}_{A,k}$ can be used as the scattering data to recover the same scatterer, now represented by the function $q^{\xi}(x, y) = q(x-a, y-b)$. According to Observation 3.5, the angular resolution provided by the scattering data $S^{\xi}_{A,k}$ is about half a wavelength. In other words, the resolution of q^{ξ} on any circle centered at ξ is about half a wavelength. Therefore, for a given point x inside the scatterer and for a given direction $\vec{\tau}$, we can always choose the center ξ which is sufficiently far from the location of the scatterer, such that there is one circle centered at ξ which passes through x in direction $\vec{\tau}$. Since the resolution of the scatterer on this circle is about half a wavelength, and since $S^{\xi}_{A,k}$ contains the same amount of information about q as the original scattering data $S_{\varpi,k}$ does, we obtain

Observation 3.6 *(Uncertainty Principle) Suppose that the smooth scatterer q has compact support $D(\varpi)$, and that $S_{\varpi,k}$ is the corresponding scattering matrix. Then it is increasingly difficult to determine from $S_{\varpi,k}$ small features of q as their sizes become decreasingly less than half a wavelength. In other words, contained in the measurements $S_{\varpi,k}$ are essentially the Fourier modes of q inside the Fourier aperture $D(N_0(2k))$.*

Remark 3.7 *The Uncertainty Principle is a reformulation of the ill-posedness of the inverse scattering problem: small features, or high-frequency modes of the scatterer are essentially non-observable in a scattering experiment. We therefore denote by $D(2k)^+$ the Fourier aperture where the Fourier modes of q can be recovered from the measurements $S_{\varpi,k}$ in a well-conditioned procedure.*

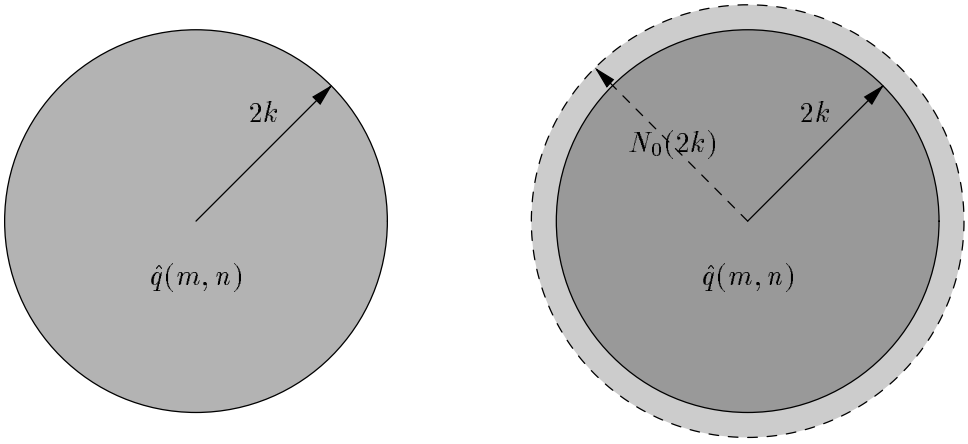

Figure 5: Fourier apertures $D(2k)$ and $D(2k)^+$.

3.4 Reformulating Scattering Problem

Denote by q_k the low-frequency part of q in the Fourier aperture $D(2k)^+$, so that

$$\widehat{(q_k)}_{m,n} = \begin{cases} \hat{q}_{m,n}, & (m,n) \in D(2k)^+, \\ 0, & (m,n) \notin D(2k)^+. \end{cases} \tag{33}$$

The goal of inversion, in the lights of Observation 3.6, is to stably obtain q_k within a reasonable precision. By definition, q_k is the only component of q that is observable in the scattering data $S_{\varpi,k}$ (see Remark 3.10). In other words, the original forward model q in (26) or (7) can be replace by q_k without essentially changing the nonlinear equation. We therefore reformulate (7) as

$$\frac{dS_{r,k}}{dr} = \frac{i\pi r}{2} k^2 (J_{kr} + S_{r,k} \cdot H_{kr}) \cdot \widehat{(q_k)}_r \cdot (H_{kr} \cdot S_{r,k} + J_{kr}). \tag{34}$$

Definition 3.8 *To a scattering experiment at frequency k, a scatterer $\check{q}$ is said to look (essentially) the same as a scatterer $\check{q}$ if they produce essentially the same scattering measurements in the experiment.*

Definition 3.9 *A forward model $\tilde{q}$ is said to be observable, or an observable part of the original scatterer q, to a scattering experiment at frequency k, if it looks the same as the original q, and its L^2 norm is the least among those that look the same as q.*

Remark 3.10 *At frequency k, q_k looks the same as the original q to a full-aperture experiment, it is also observable to the full-aperture experiment. On the other hand, in an experiment of limited aperture, q_k may not be the observable forward model, but it looks the same as the observable.*

3.5 Continuity of q_k in Frequency k

In this subsection, we argue that q_k, the observable part of q at frequency k, depends on k continuously. This is certainly true in the special case of small q. There, the

observable part of q consists of its Fourier modes in the aperture $D(2k)$. Therefore, new Fourier modes added to $q_{k+\delta k}$ are those $\hat{q}_{m,n}$ in the annulus

$$A(k,\delta k) = \{\ (m,n),\ 2k \le \sqrt{m^2+n^2} \le 2(k+\delta k)\ \}. \tag{35}$$

Consequently, the perturbation in q_k, due to the small perturbation in k, is small:

$$\|q_{k+\delta k} - q_k\|_2 = \|\widehat{q_{k+\delta k}} - \widehat{q_k}\|_2 = \int_{A(k,\delta k)} \hat{q}_{m,n} \cdot dm \cdot dn = O(\delta k). \tag{36}$$

Assuming the well-posedness of the initial value problem (see (7), (6)) of the Riccati equation, we further argue that the dependence of q_k on k is also continuous in the general case where q is not small. This well-posedness means, in particular, that the entries of the scattering matrix $S_{r,k}$ is a smooth function of k; therefore the amount of information the process (28) acquires from q depends on k smoothly. We summarize the above discussion for later reference.

Observation 3.11 *To a full-aperture experiment, the observable forward model q_k depends continuously on k in the L^2 norm.*

We wish to carry this point further to the case of limited-aperture measurements. Denote by $q_{k,l}$ the observable part of q corresponding to an experiment of a limited aperture. Usually, $q_{k,l}$ is not the same as q_k, and therefore, due to Definition 3.9,

$$\|q_{k,l}\|_2 < \|q_k\|_2. \tag{37}$$

We postulate that Observation 3.11 is still valid for scattering experiments with limited aperture.

3.6 A Recursive Linearization Algorithm

Suppose that a set of full-aperture, full-bandwidth scattering data (see (3)) are given, we present in this subsection a stable method for the solution of the inverse scattering problem. There are two approaches to the description of the method: one is based on the Lippmann-Schwinger equation (see [12]), the other on the Riccati equation, which has been numerically implemented (see Section 4), and which is the one we present here. Consider the nonlinear mapping which maps the scatterer q to the scattering data defined by (27) or by the initial value problem (34) and (6). For $k = k_1,\ k_2,\ \ldots$ (see Figure 6), we describe a procedure which recursively determines q_k at $k = k_j$ for

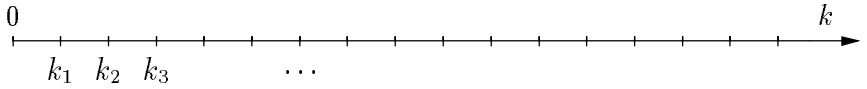

Figure 6: Computational Grid in the Frequency Space.

$j = 1, 2, \ldots$ Indeed, for sufficiently small k_1, the relation between q_{k_1} and S_{r,k_1} becomes

essentially linear (see Section 3.1), and the problem (34), (6) can be replaced by the linear one (see Lemma 3.4):

$$S'_{r,k_1} = \frac{i\pi r}{2} k_1^2 \cdot J_{k_1 r} \cdot \widehat{(q_{k_1})}_r \cdot J_{k_1 r} \tag{38}$$

$$S_{0,k_1} = 0 \tag{39}$$

The solution to this linear initial value problem is obviously given by the formula

$$S_{\varpi,k_1} = \frac{i\pi k_1^2}{2} \int_0^{\varpi} J_{k_1 r} \cdot \widehat{(q_{k_1})}_r \cdot J_{k_1 r} \cdot r \cdot dr. \tag{40}$$

Now for the given scattering data S_{ϖ,k_1}, the scatterer q_{k_1} can be obtained by solving the linear problem (40).

Suppose now that the scatter $q_{\tilde{k}}$ have heen recovered at some $\tilde{k} > 0$, and that $k > 0$

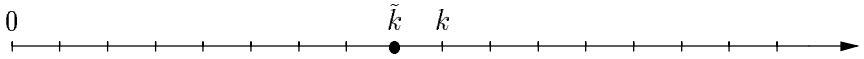

Figure 7: Update from $\tilde{k}$ to k.

is slightly greater than $\tilde{k}$. We wish to determine q_k, or equivalently, to determine the perturbation

$$\delta q = q_k - q_{\tilde{k}}. \tag{41}$$

This can be achieved by employing a standard perturbational analysis on the parameter k (see, e.g., Section 2.6 in [13]); we solve at the frequency k the forward scattering problem

$$\check{S}'_{r,k} = \frac{i\pi r}{2} k^2 (J_{kr} + \check{S}_{r,k} \cdot H_{kr}) \cdot \widehat{(q_{\tilde{k}})}_r \cdot (H_{kr} \cdot \check{S}_{r,k} + J_{kr}), \tag{42}$$

$$\check{S}_{0,k} = 0, \tag{43}$$

corresponding to the scatterer $q_{\tilde{k}}$. As a result of the forward solve, we obtain $\check{S}_{r,k}$ for all $r \in [0, \varpi]$, which will be used later in the linearized equations for the perturbation δq (see equations (46), (48)).

Remark 3.12 *On the assumption that the initial value problem of the Riccati equation (see (6), (7)) is well-posed, we observe that the scattering matrix $\check{S}_{r,k}$, the solution of (42) and (43) with the scatterer function $q_{\tilde{k}}$, is different from but close to $S_{r,k}$; for the latter is the solution of the same equations*

$$S'_{r,k} = \frac{i\pi r}{2} k^2 (J_{kr} + S_{r,k} \cdot H_{kr}) \cdot \widehat{(q_k)}_r \cdot (H_{kr} \cdot S_{r,k} + J_{kr}), \tag{44}$$

$$S_{0,k} = 0, \tag{45}$$

with a different scatterer function q_k close to $q_{\tilde{k}}$.

Subtracting (42) from (44), and omitting the second order smallness in δq and in $(\delta S)_{r,k} = S_{r,k} - \check{S}_{r,k}$, we obtain the linear ordinary differential equation

$$\begin{aligned}(\delta S)'_{r,k} &= \frac{i\pi r}{2}k^2 \Big\{(J_{kr} + \check{S}_{r,k}\cdot H_{kr})\cdot\widehat{(q_{\tilde{k}})}_r\cdot H_{kr}\cdot(\delta S)_{r,k} + \\ &\quad + (\delta S)_{r,k}\cdot H_{kr}\cdot\widehat{(q_{\tilde{k}})}_r\cdot(H_{kr}\cdot\check{S}_{r,k} + J_{kr}) + \\ &\quad + (J_{kr} + \check{S}_{r,k}\cdot H_{kr})\cdot\widehat{(\delta q)}_r\cdot(H_{kr}\cdot\check{S}_{r,k} + J_{kr})\Big\} \qquad (46)\end{aligned}$$

for δS, with its initial value

$$(\delta S)_{0,k} = 0. \qquad (47)$$

According to Lemma A.5, the linear initial value problem (46), (47) has the formal solution

$$\begin{aligned}(\delta S)_{r,k} &= \frac{i\pi}{2}k^2\int_0^r E_L(\tau, r; P_y)\cdot(J_{k\tau} + \check{S}_{\tau,k}\cdot H_{k\tau})\times \\ &\quad \widehat{(\delta q)}_\tau\cdot(H_{k\tau}\cdot\check{S}_{\tau,k} + J_{k\tau})\cdot E_R(\tau, r; P_x)\cdot\tau\cdot d\tau \qquad (48)\end{aligned}$$

where $P_x(r) : X_{kr} \mapsto X_{kr}$, $P_y(r) : Y_{kr} \mapsto Y_{kr}$ are defined by the formulae

$$P_x(r) = \frac{i\pi}{2}k^2 r H_{kr}\cdot\widehat{(q_{\tilde{k}})}_r\cdot(H_{kr}\cdot\check{S}_{r,k} + J_{kr}), \qquad (49)$$

$$P_y(r) = \frac{i\pi}{2}k^2 r(J_{kr} + \check{S}_{r,k}\cdot H_{kr})\cdot\widehat{(q_{\tilde{k}})}_r\cdot H_{kr}. \qquad (50)$$

In particular, at $r = \varpi$, (48) becomes a system of linear equations for $\widehat{\delta q}$:

$$\begin{aligned}&\frac{i\pi}{2}k^2\int_0^\varpi E_L(r, \varpi; P_y)\cdot(J_{kr} + \check{S}_{r,k}\cdot H_{kr})\cdot\widehat{(\delta q)}_r\times \\ &(H_{kr}\cdot\check{S}_{r,k} + J_{kr})\cdot E_R(r, \varpi; P_x)\cdot r\cdot dr = (\delta S)_{\varpi,k}, \qquad (51)\end{aligned}$$

with the right hand sides $(\delta S)_{\varpi,k}$ given, and the coefficients $E_L, E_R, \check{S}$ known. Denote by $L(X_{k\varpi} \mapsto Y_{k\varpi})$ the linear space of all linear mappings from $X_{k\varpi}$ to $Y_{k\varpi}$, and by $\mathcal{L}_k : L^2[D(\varpi)] \mapsto L(X_{k\varpi} \mapsto Y_{k\varpi})$ the linear operator defined by (51). The linear equation (51) can be rewritten as

$$\mathcal{L}_k(\delta q) = (\delta S)_{\varpi,k}. \qquad (52)$$

The linear equations can be solved (see Remark 3.13) for δq, and the scatterer q_k can be obtained from the previously recovered scatterer $q_{\tilde{k}}$ via (41).

Remark 3.13 *The rank of the linear operator $\mathcal{L}_k$ is essentially finite due to the ill-posedness of the inverse scattering problem (see Observation 3.6 and Remark 3.7). Therefore, (52) is solved as a least-squares problem of finite dimensions to yield the solution δq. Our numerical experiments show that in fact only a rough approximation to q_k is required to maintain a stable recursion in k.*

4 Implementations of the Recursive Procedure

In this section, we discuss the discretization of the spatial variables (r, θ), the treatment of the scattering matrix S, the numerical computation of the Riccati equation (42), the evaluation of the linear operators E_L, E_R, the formation of the linear system (51), and the least-squares solution of it.

4.1 Discretizing the Independent Variables (r, θ)

4.1.1 Discretizing the Azimuth θ

Given a radius $r > 0$ and an even number $N > 0$, we denote by

$$\{ (r, \theta_l) \mid \theta_l = \frac{2l\pi}{N} \} \tag{53}$$

the equispaced points on the circle $\{ (r, \theta) \mid \theta \in [0, 2\pi] \}$ (the value of N will be specified later in this subsection), so that functions on the circle are represented by their values at these points. In particular, the scatterer q and its perturbation δq on the circle are understood as real valued vectors of dimension N; the linear diagonal operator q_r (see Remark A.3) is now a diagonal matrix of dimension N; the Fourier transform F and its inverse F^{-1} are understood as the discrete Fourier transforms (DFT) of dimension N; and the linear operator $\hat{q}_r$ (see (100)) is regarded as a matrix of dimension N. A sequence $\alpha = \{\alpha_m\} \in X_{kr}$ is truncated and rearranged in the DFT order

$$\{ \alpha_0, \alpha_1, \ldots, \alpha_{N/2}, \alpha_{-N/2+1}, \ldots, \alpha_{-1} \}; \tag{54}$$

so truncated and rearranged are the vectors in Y_{kr}, the matrices J_{kr}, H_{kr} and $S_{r,k}$. We will refer to the central entries of the vector (54) as the high-frequency entries. The high-frequency entries of the scattering matrix are those in the center rows and columns. A vector

$$\{ \beta_0, \beta_1, \ldots, \beta_{M/2}, \beta_{-M/2+1}, \ldots, \beta_{-1} \} \tag{55}$$

of dimension $M < N$ (M even) can be added to α by firstly zero padding β

$$\{ \beta_0, \beta_1, \ldots, \beta_{M/2}, 0, \ldots 0, \beta_{-M/2+1}, \ldots, \beta_{-1} \}, \tag{56}$$

and then carrying out the regular addition of two vectors of the same size. Similarly, a scattering matrix of dimension M can be viewed as of dimension N by zero padding.

Remark 4.1 *When matrices of different dimensions appear in an arithmetic operation (see, for example, (76)), the smaller matrices are first zero padded to the maximum dimension; the final result is a matrix of the maximum dimension.*

In the rest of this paper, we denote by $n_\theta(r) = N$. Numerical experiments show that $n_\theta(r)$ can be chosen between $2rk$ and $3rk$, which is to say, 2 to 3 points per wavelength along the arclength of the circle $|x| = r$. In our numerical experiments,

$$n_\theta(r) \geq 2.8rk. \tag{57}$$

4.1.2 Discretizing the Radius r

Over the interval $[0, \varpi]$, we employ two sets of equispaced computational grids:

$$\{\ r_j = j{\cdot}h_r,\ \ j \ = \ 0, 1, \ldots, n_r,\ \ h_r = \frac{\varpi}{n_r}\ \}, \tag{58}$$

$$\{\ \rho_m = m{\cdot}h_\rho,\ \ m \ = \ 0, 1, \ldots, n_\rho,\ \ h_\rho = \frac{\varpi}{n_\rho}\ \}, \tag{59}$$

with integers $n_r > n_\rho$. The first set of grid is used for the solution of initial value problem (42) and (43). The second set is for discretization of the integral in equation (51). Our experiments show that, with the second order ODE solver of Section 4.2,

$$n_r \sim 10\frac{k\varpi}{\pi}, \tag{60}$$

namely, the grid is about ten points per wavelength over the interval $[0, \varpi]$. For convenience in computation, the ratio n_r/n_ρ is chosen as an integer, so that

$$\{\ \rho_m\ \} \subset \{\ r_j\ \}. \tag{61}$$

The ratio is 2 or 3 in our numerical experiments.

4.2 Solving the Forward Scattering Problem

The initial value problem (42) and (43) of the Riccati equation is solved by an second order, implicit, alternating scheme. Assuming that j is the step counter, we initially set $j = 0$, $r = 0$, and $\check{S}_{0,k} = 0$. For $j = 1, 2, \ldots, n_r$, $\check{S}$ is updated from r_{j-1} to r_j by the following procedures (with $\tau = (r_j + r_{j-1})/2$):

$$\begin{aligned} \check{S}_{r_j,k} - \check{S}_{r_{j-1},k} \ &= \ h_r\frac{i\pi\tau}{2}k^2(J_{kr_{j-1}} + \check{S}_{r_{j-1},k}{\cdot}H_{kr_{j-1}})\times \\ &\quad \widehat{(q_{\tilde{k}})}_\tau{\cdot}(J_{kr_j} + H_{kr_j}{\cdot}\check{S}_{r_j,k}),\ j\text{odd}; \end{aligned} \tag{62}$$

$$\begin{aligned} \check{S}_{r_j,k} - \check{S}_{r_{j-1},k} \ &= \ h_r\frac{i\pi\tau}{2}k^2(J_{kr_j} + \check{S}_{r_j,k}{\cdot}H_{kr_j})\times \\ &\quad \widehat{(q_{\tilde{k}})}_\tau{\cdot}(J_{kr_{j-1}} + H_{kr_{j-1}}{\cdot}\check{S}_{r_{j-1},k}),\ j\text{even}. \end{aligned} \tag{63}$$

For each r_j, it requires $O\left(N_\theta^3(r_j)\right)$ operations to solve each of the linear systems (63), (63). Since there are n_r steps over $[0, \varpi]$ in the ODE solve, and since n_r, n_θ are both proportional to N_w (see (57), (60), and Remark 2.1), the total cost for solving the Riccati equation is $O(N_w^4)$.

4.3 Evaluating the Operators E_L, E_R

In this subsection, we discretize the linear equation (51) and evaluate E_L, E_R on the grid $\{\rho_m\}$. There are several ways to evaluate the matrices E_L, E_R; here, we present one of them. For convenience discussion, we first scale the linear system (51) using

formulae (104), (105): multiplying (51) from the left by $E_L(\varpi, 0; P_y)$, and from the right by $E_R(\varpi, 0; P_x)$, we obtain

$$\begin{aligned} & \frac{i\pi}{2} k^2 \int_0^{\varpi} E_L(r, 0; P_y) \cdot (J_{kr} + \check{S}_{r,k} \cdot H_{kr}) \cdot \widehat{(\delta q)}_r \times \\ & (H_{kr} \cdot \check{S}_{r,k} + J_{kr}) \cdot E_R(r, 0; P_x) \cdot r \cdot dr \\ = \quad & E_L(\varpi, 0; P_y) \cdot (\delta S)_{\varpi,k} \cdot E_R(\varpi, 0; P_x). \end{aligned} \tag{64}$$

The integration over $[0, \varpi]$ in (51) is discretized using the trapezoidal rule on the equispaced grids $\{\rho_m\}$:

$$\begin{aligned} & \frac{i\pi}{2} k^2 h_\rho \sum_{j=0}^{n_\rho} \tilde{\rho_j} E_L(\rho_j, 0; P_y) \cdot (J_{k\rho_j} + \check{S}_{\rho_j,k} \cdot H_{k\rho_j}) \times \\ & \widehat{(\delta q)}_{\rho_j} \cdot (H_{k\rho_j} \cdot \check{S}_{\rho_j,k} + J_{k\rho_j}) \cdot E_R(\rho_j, 0; P_x) \\ = \quad & E_L(\varpi, 0; P_y) \cdot (\delta S)_{\varpi,k} \cdot E_R(\varpi, 0; P_x). \end{aligned} \tag{65}$$

where $\tilde{\rho_j}$ is defined as

$$\tilde{\rho_j} = \begin{cases} \rho_j & j = 1, 2, \ldots, n_\rho - 1, \\ \rho_j / 2 & j = 0, n_\rho \ . \end{cases} \tag{66}$$

Although the two matrices $E_L(r, 0; P_y)$, $E_R(r, 0; P_x)$ are required at the coarser grid $r = \rho_m$, they will be first obtained on the finer grid $r = r_j$ in order to maintain an accuracy comparable to that in which the scattering matrix $\check{S}$ is obtained. At $r = r_j$, $j = 1, 2, \ldots$, $E_L(r, 0; P_y)$, $E_R(r, 0; P_x)$ can be calculated recursively (see [13], Section 4.3 for further details), starting with the initial values

$$E_L(0, 0; P_y) = I, \tag{67}$$

$$E_R(0, 0; P_x) = I. \tag{68}$$

For $j = 1, 2, \ldots, n_r$, the matrix $E_L(r_j, 0; P_y)$ is updated from $E_L(r_{j-1}, 0; P_y)$ via the formula

$$E_L(r_j, 0; P_y) = E_L(r_{j-1}, 0; P_y) \left(I - \frac{h_r}{2} P_y(r_{j-1}) \right) \left(I + \frac{h_r}{2} P_y(r_j) \right)^{-1}; \tag{69}$$

the matrix $E_R(r_j, 0; P_x)$ is updated from $E_R(r_{j-1}, 0; P_x)$ via the formula

$$E_R(r_j, 0; P_x) = \left(I + \frac{h_r}{2} P_x(r_j) \right)^{-1} \left(I - \frac{h_r}{2} P_x(r_{j-1}) \right) E_R(r_{j-1}, 0; P_x). \tag{70}$$

4.4 Forming the Linear Equations

With $E_L(r_j, 0; P_y)$, $E_R(r_j, 0; P_x)$ evaluated (see Section 4.3), and $\check{S}_{r_j,k}$ obtained from the forward solve (see Section 4.2), we can explicitly write the linear system (65) in terms of these matrices in order to solve it.

For $j = 1, 2, \ldots, n_\rho$, we denote by (see Section 4.1.1) $N_j = n_\theta(\rho_j)$ the number of equispaced points on the circle $r = \rho_j$, which is also the dimension of the matrices $\check{S}_{\rho_j,k}$, $E_L(\rho_j, 0; P_y)$, and $E_R(\rho_j, 0; P_x)$. Given j and for $0 \leq m < N_j$, we further denote by $\theta_{j,m} = 2m\pi/N_j$ the azimuthal values of the equispaced points on the circle $r = \rho_j$. Finally, for a smooth function g, we denote by $g_{j,m}$ the values of g at the equispaced points on the circle. We will require the matrix $dS = (\delta S)_{\varpi,k}$ of dimension N_{n_ρ}, and the three matrices of dimension N_j

$$B_j = E_L(\rho_j, 0; P_y)\cdot(J_{k\rho_j} + \check{S}_{\rho_j,k} H_{k\rho_j})\cdot(N_j^{\frac{1}{2}} F), \tag{71}$$

$$A_j = (N_j^{\frac{1}{2}} F^{-1})\cdot(J_{k\rho_j} + H_{k\rho_j}\check{S}_{\rho_j,k})\cdot E_R(\rho_j, 0; P_x), \tag{72}$$

$$(\delta q)_j = diag\{\ (\delta q)_{j,0}, (\delta q)_{j,1}, \ldots, (\delta q)_{j,N_j}\ \}, \tag{73}$$

where $N_j^{\frac{1}{2}} F$ and $N_j^{\frac{1}{2}} F^{-1}$ are scaled discrete forward and backward Fourier transforms, so that

$$(N_j^{\frac{1}{2}} F)_{m,n} = \exp(-i2mn\pi/N_j), \tag{74}$$

$$(N_j^{\frac{1}{2}} F^{-1})_{m,n} = \exp(i2mn\pi/N_j). \tag{75}$$

It follows from (100) that (65) becomes

$$\frac{i\pi}{2} k^2 h_\rho \cdot E_L(0, \varpi; P_y)\cdot \left(\sum_{j=0}^{n_\rho} \frac{\tilde{\rho}_j}{N_j}\cdot B_j\cdot(\delta q)_j\cdot A_j \right) \cdot E_R(0, \varpi; P_x) = dS, \tag{76}$$

Denoting by $\mathcal{D}$ the linear space of real-valued vectors of dimension $N_q = \sum_{j=1}^{n_\rho} N_j$, and by $\mathcal{R}$ the linear space of dimension $N_s = N_{n_\rho}^2$, we observe that $dS \in \mathcal{R}$, that (76) is a system of linear equations for the vector $\delta q \in \mathcal{D}$ defined by

$$\begin{aligned} \delta q = \{\quad & ((\delta q)_{1,0}, (\delta q)_{1,1}, \ldots, (\delta q)_{1,N_1-1}), \\ & ((\delta q)_{2,0}, (\delta q)_{2,1}, \ldots, (\delta q)_{2,N_2-1}), \\ & \ldots, \\ & ((\delta q)_{n_\rho,0}, (\delta q)_{n_\rho,1}, \ldots, (\delta q)_{n_\rho,N_{n_\rho}-1})\ \}^T, \end{aligned} \tag{77}$$

and that (76) defines a linear operator $\mathcal{A} : \mathcal{D} \mapsto \mathcal{R}$ so that

$$\mathcal{A}\ (\delta q) = dS. \tag{78}$$

Remark 4.2 *The procedures for computing* $\{\ A_j,\ B_j,\ j = 1, 2, \ldots, n_\rho\ \}$, *as well as the application of* $\mathcal{A}$ *to a vector, cost* $O(N_w^4)$ *arithmetic operations.*

Remark 4.3 *The inner product in* $\mathcal{R}$ *is define by* $(u, v) = \sum_{j=1}^{N_s} u_j\cdot v_j$ *so that the induced norm for* $\mathcal{R}$ *is the standard* L^2 *norm. Since vectors in* $\mathcal{D}$ *of the form (77) represent functions of* $L^2(D(\varpi))$ *in polar coordinates, and since the inner product of a pair of such functions in* $L^2(D(\varpi))$ *defined by the formula*

$$(f, g) = \int_0^\varpi \left(\frac{1}{2\pi} \int_0^{2\pi} \overline{f(r,\theta)}\cdot g(r,\theta) d\theta \right) \cdot r \cdot dr \tag{79}$$

induces the L^2 norm, we define the discrete version of (79) by the formula

$$(x, y)_{polar} = h_\rho \sum_{j=0}^{n_\rho} \tilde{\rho}_j \left(\frac{1}{N_j} \sum_{m=0}^{N_j-1} \overline{x}_{j,m} y_{j,m} \right), \tag{80}$$

as the inner product for the vectors $x,\ y \in \mathcal{D}$. We refer to the norm of $\mathcal{D}$ induced by (79) as the ℓ^2_{polar} norm.

4.5 Least-square Solution of the Linearized Equation

In order to solve the least-squares problem (78), the conjugate-gradient method was employed (to the normal equation of (78)) because it is the least expansive among several standard methods, including QR decomposition, Gram-Schmidt orthogonalization. The application of the conjugate-gradient method in this case is straightforward and tedious with one exception: the inner product (80) must be used (see Remark 4.3) to obtain the solution in $\mathcal{D}$ with the least ℓ^2_{polar} norm. It means that the inner product in a standard conjugate-gradient method must be replaced with (80), and that the adjoint operator of $\mathcal{A}$ is understood as follows. We denote by A a matrix of dimension $N_s \times N_q$ whose i-th row, $a^{(i)}$, is such that

$$\left(\left[a^{(i)} \right]^*,\ y \right)_{polar} = \left[\mathcal{A}\ (y) \right]_i \tag{81}$$

for all $y \in \mathcal{D}$. Obviously, the Hermitian of A, namely, the linear operator $A^* : \mathcal{R} \mapsto \mathcal{D}$, is the adjoint operator of $\mathcal{A}$, with respect to the inner products in $\mathcal{R}$ and $\mathcal{D}$. With $\delta q = A^* u$, it is a tedious but straightforward manipulation to verify that

$$\overline{(\delta q)_{j,m}} = \frac{ik^2}{4} \sum_{n,l=1}^{N_j} \{A_j\}_{m,n} \cdot \{B_j\}_{l,m} \cdot \{\ E_R(0, \varpi; P_x) \cdot u^* \cdot E_L(0, \varpi; P_y)\ \}_{n,l} \tag{82}$$

where $u \in \mathcal{R}$ is understood as an $N_s \times N_s$ matrix.

Remark 4.4 *It is easy to see from (82) that the application of $\mathcal{A}^*$ to a vector cost $O(N_w^4)$ arithmetic operations (see also Remark 4.2).*

Remark 4.5 *Since only an approximate solution of the least-squares is required (see Remark 3.13), the conjugate-gradient iteration is usually terminated at n-th step in our numerical experiments when the ratio of norms of the last and the initial residuals*

$$\sigma = \frac{\|r_n\|}{\|r_0\|} \tag{83}$$

is about 10^{-3}.

5 Numerical Results and Discussions

FORTRAN programs were written implementing the procedures described in the preceding section. In this section, to illustrate the performance of the algorithm, we present several numerical examples for the inversion of the Helmholtz equation in two dimensions. Remarks will be made, at the beginning and the end of this section, to discuss some technical details of the numerical experiments.

5.1 The Recursion in k and the Complexity

Our numerical experiments show that frequently k_j (see Figure 7) can be chosen such that the size of the scatterer is about j wavelengths. For instance, we may set $k_j = j$ for a scatterer not large in magnitude inside a disk of diameter 2π.

Assuming a finite number of iterations are required in the conjugate gradient method, for the linear system (52) needs not be solved accurately according to Remark 3.13, we observe that the least-squares solution of (52) can be approximately obtained at a cost of $O(N_w^4)$ arithmetic operations (see Remarks 4.2, 4.4). Then, the inversion algorithm requires $O(N_w^5)$ operations since there are about N_w frequencies employed in the recursion.

5.2 The Forward Modeling

The scattering data (see Section 2.2) are obtained by numerical solution of the forward scattering problem—the initial value problem of the Riccati equations (see (7) and (6)). In our numerical computation, we assume the scatterer q is nonzero in a disk of radius $\varpi = \pi$.

We used the standard fourth order Runge-Kutta method and the second order implicit scheme described in Section 4.2 for the numerical solution of the ordinary differential equation (7). In the numerical reconstructions presented below, the scattering data used were obtained with an accuracy 10^{-3} to 10^{-4}.

5.3 Numerical Examples

A large number of numerical experiments have heen made in which several types of the scatterers have been reconstructed. The reconstructions of three types of scatterers are presented here.

Example 1: Reconstruct a scatterer defined by

$$\begin{aligned} q_1(x,y) &= 0.15\cdot(1-x)^2\cdot e^{-(x^2+(y+1)^2)} - 0.5\cdot\left(\frac{x}{5} - x^3 - y^5\right)\cdot e^{-(x^2+y^2)} \\ &\quad - \frac{1}{60}\cdot e^{-((x+1)^2-y^2)}, \end{aligned} \tag{84}$$

inside the disk $D(\pi)$; see Figure 8 for surface and contour plots of the scatterer function. Nine frequencies were used in the reconstruction, corresponding to wave numbers $k = 1, 2, \cdots, 9$. The inversion algorithm reconstructed it accurately (the reconstructed

k	1	2	3	4	5	6	7	8	9
e_2	0.57	0.41	0.16	3.1-2	6.4E-3	2.2E-3	1.2E-3	7.9E-4	5.6E-4

Table 1: L^2 Error of Reconstruction at 9 Frequencies, Example 1.

function will not be plotted against the exact since the error is so small that it is invisible in the plot). The procedure cost 122 seconds CPU time on a Cray C-90 computer; see Table 1 for the L^2 error of the reconstruction.

Example 1.1: To test the stability of the algorithm, we reconstruct in this example the scatterer q_1 but with noisy data. Noise is added to the scattering data used in Example 1 by truncating each number in the data to certain digits. For instance, truncating the number 0.129876 to two digits yields 0.12, and the perturbation (or noise) incurred here by the truncation is about 1%. Three tests were made here corresponding to truncations of the scattering data to $N_d = 3,\ 2,\ 1$ digits. The resulting errors in the inversion are listed in Table 2.

Figure 9 shows the surface and contour plots of the reconstruction with the scattering data truncated to one digit, namely, the noisy data used here only have one-digit accuracy. This is a quite severe test to an algorithm. This time, not only our computation didn't blow up, it actually reconstructed the scatterer with a 11% error. Stability tests were also performed to other scatterers whose reconstructions are presented in this paper, the results being similar.

Example 2: Reconstruct a scatterer defined by

$$q_2(x, y) = 0.2\left\{1 + \cos(11{\cdot}x) + \sin(11{\cdot}y)\right\}, \tag{85}$$

inside $D(\pi)$; see Figure 10 for surface and contour plots of the scatterer. This is a quite oscillatory function. Inside the disk, there are about 160 peaks and valleys representing a highly rugged index of refraction. The computation simulates an acoustic experiment in which the background speed of sound is that of water; the scatterer is 20.87 centimeters in diameter (about the size of a human head). Nine frequencies, $f = 7, 14, 21, \cdots, 63$ kHz, were used in the reconstruction, corresponding to wave numbers $k = 1, 2, \cdots, 9$. At $f = 63$ kHz, 108 transducers were required around the scatterer. The procedure cost 122 seconds CPU time on a Cray C-90 computer; see Table 3 for the L^2 error of the reconstruction. Because of the complicated structure of the scatterer, the reconstructed scatterer is plotted against the exact scatterer first horizontally across the diameter of the disk $D(\pi)$, then across concentric circles of various radii between 0 and π of the disk; see Figures 11, 12.

N_d	3	2	1
e_2	1.4E-3	1.3E-2	1.1E-1

Table 2: L^2 Error of Reconstruction with Noisy Data, Example 1.1.

k	1	2	3	4	5	6	7	8	9
e_2	0.53	0.56	0.56	0.55	0.25	8.2E-2	3.6E-2	1.9E-2	1.2E-2

Table 3: L^2 Error of Reconstruction at 9 Frequencies, Example 2.

Example 3: Reconstruct a scatterer defined in $D(\pi)$ by

$$q_3(x,y) = \begin{cases} q_1(x/0.8, y/0.8) & \text{if } r < 2.6, \\ -0.5 & \text{if } r \in [2.6, 2.9), \\ 0 & \text{if } r \geq 2.9; \end{cases} \tag{86}$$

see Figure 13 for surface and contour plots of the function. This scatterer is difficult to reconstruct for two reasons.

(1) Across the two circles $r = 2.6$ and $r = 2.9$, the function is discontinuous. The value of the function changes sharply to -0.5 in the narrow annulus.

(2) If the background speed of sound is that of water, then the material in the narrow band $2.6 \leq r \leq 2.9$ has speed of sound 1.4 times as large as that of water. As a result, this high-speed region with sharp boundaries blocks the passage of the probing sound waves to the inside of the structure, making it hard to reconstruct the smooth part of the scatterer in the middle of the object.

This example could be regarded as a model problem for ultrasound tomography of a human head, where the skull is represented by the thin layer of denser material in the region $2.6 \leq r \leq 2.9$. If the actual object is 20.87 centimeters in diameter, the frequencies used were $f = 7, 14, 21, \cdots, 84$ kHz, corresponding to wave numbers $k = 1, 2, \cdots, 12$. At $f = 84$ kHz, 128 transducers were used around the scatterer. The CPU time required for the procedure was 263 seconds on a Cray C-90 computer. The

k	1	2	3	4	5	6
e_2	0.576	0.510	0.367	0.260	0.231	0.220
k	7	8	9	10	11	12
e_2	0.197	0.164	0.146	0.141	0.138	0.136

Table 4: L^2 Error of Reconstruction at 12 Frequencies, Example 3.

L^2 errors of the reconstruction at the 12 frequencies are listed in Table 3. Figure 14 shows the surface and contour plots of the reconstructed scatterer, whereas Figure 15 shows the reconstruction horizontally across the diameter of the scatterer.
An examination of the plots show that the error of the reconstructions occurs largely around the discontinuities, while the smooth part is recovered more accurately.

5.4 Discussions and Conclusions

The following technical details of the numerical implementation appear to be worthy mentioning.

1. The convergence of recursive linearization procedure depends, of course, on the step size of the frequency k. We find in our numerical experiments that when the scatterer function is not large (for example, when $-0.8 \leq q \leq 1$), convergence is usually guaranteed with the step size given by $k_j = j$. In general, smaller step sizes are required when the scatterer function is very large or very closed to -1.

On the other hand, larger step sizes of k can generally be used at higher frequencies k without affecting the convergence. This is so because at a relatively high frequency $k = a$ where the dominant lower-frequency components of the scatterer have been recovered, $q - q_a$ is small. Therefore, the perturbation $\delta q = q_b - q_a$ will be small for a relatively large step size of $\delta k = b - a$.

2. The stability of the algorithm is not sensitive to the step size of the frequency k. It is largely controlled by the way the ill-posed linear system (52) is solved. Numerical experiments show that the up-recursion in frequency k is usually unstable when the least-squares solution of (52) is obtained in such a precision that σ (see (83)) is smaller than 10^{-6}. With scattering data accurate to three digits, we find that $\sigma = 10^{-3}$ (see Remark 4.5) is suitable to inversion in a varieties of cases.

The following discussions are about the models of forward scattering.

3. The use of cylindrical geometry to introduce the scattering matrix, and subsequently, to obtain the Riccati equation, is a convenient but not the only approach to the forward modeling. Scattering matrix associated with straight-line geometry, and its Riccati equation, for example, are introduced in [10].

4. Forward models other than the Riccati equations can be used to recursively linearize the inverse problem. The Lippmann-Schwinger equation seems a better candidate for the forward modeling because there is a recursive procedure that solves accurately the forward problem in $O(N_w^3)$ operations at a frequency. Thus, the multi-frequency inversion costs about $O(N_w^4)$ operations. The linearization procedure based on the Lippmann-Schwinger equation is described in [12]. Its implementation and numerical results will be reported on a later date.

The following discussions are about extensions of the algorithm to three dimensions and to other types of scattering problems.

5. The direct extension of the recursive linearization procedure to three dimensions is straightforward, but is difficult to be implemented numerically, for the procedure requires $O(N_w^8)$ operations. The high computational cost in three dimensions is primarily a result of the so-called data redundancy: at a frequency $k > 0$, the full-aperture scattering data depend on four independent parameters whereas the scatterer q to be recovered is a function of three spatial parameters. There are several ways to reduce the cost to $O(N_w^6)$; each of which uses part of the full-aperture scattering data.

6. The recursive procedure can be applied to measurements of limited aperture (see [12] for more details). In two dimensions, this only allows us to recover partial information of the scatterer within the Fourier aperture $D(2k)^+$. In three dimensions,

measurements of limited aperture may provide the same amount of information about the scatterer as do the full-aperture measurements.

7. The scheme can be used to solve inverse scattering problems of more complicated equations describing more realistic processes of acoustic, elastic, or electromagnetic scattering in which the Heisenberg's Uncertainty Principle holds. The exact formulation of the uncertainty principle may differ in specific environments, but it is certain that in the realm of wave phenomena an incident wave of a lower frequency interacts weakly with the Fourier modes of the scatterer of higher frequencies, and such an interaction produces a weaker scattered field.

8. Heisenberg's Uncertainty Principle is also valid in the case of obstacle scattering. There, lower-frequency incident fields interacts weakly with the higher-frequency roughness of the surface of the scattering obstacle. Therefore, the inverse obstacle scattering problem can be recursively linearized by the same mechanism introduced here in this paper.

9. There is the obvious need of a fast forward solver in order to speed up the computation for the inversion algorithm.

ACKNOWLEDGMENT The author wishes to thank Professor V. Rokhlin for his advice and help thoughout this project, and to thank Professors R. Coifman, G. Beylkin for their useful comments and constant interests in this work.

References

[1] Eyges, L. (1972), *The Classical Eletromagnetic Field,* Dover, New York.

[2] N. Bleistein (1984), *Mathematical Methods for Wave Phenomena,* Academic Press, New York.

[3] Abramowitz, M., and Stegun, I. (1965), *Handbook of Mathematical Functions,* Dover, New York.

[4] G. Matviyenko (1992), *On the Evaluation of Bessel Functions,* Research Report 903, Department of Computer Science, Yale University.

[5] G. N. Watson (1958), *A Treatise on the Theory of the Bessel functions,* Cambridge University Press, Cambridge.

[6] D. Colton and R. Kress (1992), *Inverse Acoustic and Electromagnetic Scattering Theory,* Springer-Verlag Berlin Heidelberg.

[7] V. Rokhlin (1990), *Rapid Solution of Integral Equations of Scattering Theory in Two Dimensions,* Journal of Computational Physics, 86(2): 414

[8] G. Beylkin and R. Burridge (1990), *Linearized Inverse Scattering Problems in Acoustics and Elasticity, Wave Motion 12* 15–52.

[9] J. Sylvester (1992), *A Convergent Layer Stripping Algorithm for the Radially Symmetric Impedance Tomography Problem, Communications in PDE* **17**, No.12, pp.1955–1994.

[10] Y. Chen (1992), *On the Inverse Scattering Problem for the Helmholtz Equation in One Dimension,* Research Report 913, Department of Computer Science, Yale University.

[11] Y. Chen and V. Rokhlin (1995), *On the Riccati Equations for the Scattering Matrices in two dimensions,* Technical Report 1081, Department of Computer Science, Yale University.

[12] Y. Chen (1995), *Recursive Linearization for Inverse Scattering,* Technical Report 1088, Department of Computer Science, Yale University.

[13] Y. Chen (1996), *Inverse Scattering via Heisenberg's Uncertainty Principle,* Technical Report 1091, Department of Computer Science, Yale University.

A Notation and Several Classical Results

Here, we introduce several usages of notation in this paper, and solve a linear matrix equation associated with the Riccati matrix equation.

A.1 Notation

For $r > 0$, we denote by $D(r)$ the disk of radius r centered at the origin; by ℓ^2 the linear space of sequences ξ of complex numbers with bounded sum of squares. Denote by J_m the Bessel function of the first kind of order m, by Y_m the Neumann function (or the Bessel function of the second kind) of order m, and by H_m Hankel function of the first kind of order m, so that $H_m = J_m + i \cdot Y_m$. Given a positive number z, we denote by X_z the linear space of all two-sided complex sequences $\{\alpha_m\}$ such that for some $c > 0$

$$|\alpha_m \cdot J_m(z)| < c, \tag{87}$$

for all integer m. We will denote by Y_z the linear space of all two-sided complex sequences $\{\beta_m\}$ such that for some $c > 0$

$$|\beta_m \cdot H_m(z)| < c, \tag{88}$$

for all integer m. We will denote by J_z, H_z the infinite diagonal matrices

$$J_z = diag\{\ldots, J_{-1}(z), J_0(z), J_1(z), \ldots\}, \tag{89}$$

$$H_z = diag\{\ldots, H_{-1}(z), H_0(z), H_1(z), \ldots\}, \tag{90}$$

Remark A.1 *It is well-known (see, for example, [3], [4], [5]) that once the positive number ν is greater than z, the Bessel function $J_\nu(z)$ strictly decays as ν grows, and*

that the Neumann function $Y_\nu(z)$ strictly grows as ν grows. Moreover, $J_\nu(z)$ becomes very small, and $Y_\nu(z)$ becomes very large, when ν reaches

$$N_0(z) = z + O\left(z^{\frac{1}{3}}\right). \tag{91}$$

Finally, for $\nu \geq N_0(z)$,

$$J_m(z) \sim \frac{1}{\sqrt{2\pi m}} \cdot \left(\frac{e \cdot z}{2m}\right)^m, \tag{92}$$

$$H_m(z) \sim -i \cdot \sqrt{\frac{2}{\pi m}} \cdot \left(\frac{2m}{e \cdot z}\right)^m. \tag{93}$$

A solution of the equation of the homogeneous Helmholtz equation

$$\Delta\phi_0(x,y) + k^2\phi_0(x,y) = 0 \tag{94}$$

in a bounded domain Ω is referred to as the radiation field in Ω. A radiation field ψ outside Ω is a solution of (94) there, subject to the outgoing (Sommerfeld) radiation condition

$$\lim_{r\to\infty} \sqrt{r}\left(\frac{\partial\psi}{\partial r} - ik\psi\right) = 0. \tag{95}$$

Lemma A.2 *Given $k > 0$, $r > 0$, $\phi : D(r) \mapsto \mathbb{C}$ is a radiation field in $D(r)$ if and only if there exists a sequence $\{\alpha_j\} \in Y_{kr}$ such that for $\rho < r$,*

$$\phi(\rho,\theta) = \sum_{m=-\infty}^{\infty} \alpha_m J_m(k\rho) e^{im\theta} = F_\theta^{-1} \cdot J_{k\rho} \cdot \alpha. \tag{96}$$

Furthermore, $\psi : \mathbb{R}^2 \setminus D(r) \mapsto \mathbb{C}$ is a radiation field outside $D(r)$ if and only if there exists a sequence $\{\beta_j\} \in X_{kr}$ such that for all $\rho > r$,

$$\psi(\rho,\theta) = \sum_{m=-\infty}^{\infty} \beta_m H_m(k\rho) e^{im\theta} = F_\theta^{-1} \cdot H_{k\rho} \cdot \beta. \tag{97}$$

Denote by F the Fourier transform converting a function in $L^2[0,2\pi]$ to its Fourier coefficients in ℓ^2. Let

$$\hat{g}_m(r) = \frac{1}{2\pi}\int_0^{2\pi} g(r,\theta) e^{im\theta} d\theta, \tag{98}$$

for a smooth function $g : \mathbb{R}^2 \mapsto \mathbb{C}$, and let $\hat{g}_r$ be the matrix whose (m,n)-th entry is defined by the formula $(\hat{g}_r)_{m,n} = \hat{g}_{m-n}(r)$.

Remark A.3 *Denoting by $g_r : L^2[0,2\pi] \mapsto L^2[0,2\pi]$ the diagonal linear mapping*

$$(g_r \cdot f)(\theta) = g(r,\theta) \cdot f(\theta) \tag{99}$$

for all $f \in L^2[0,2\pi]$, we can easily verify that

$$\hat{g}_r = F \cdot g_r \cdot F^{-1}. \tag{100}$$

A.2 The Solution of a Linear ODE of Matrix

Suppose that $A(r)$, $B(r)$ and $C(r)$ are three $n \times n$ matrices depending continuously on $r \in [0,1]$. Let us consider an ordinary differential equation of the form

$$S'(r) = A(r) \cdot S(r) + S(r) \cdot B(r) + C(r). \tag{101}$$

We now wish to express in close form the solution $S(r)$ at an arbitrary $r \in (0,1]$ for prescribed initial value $S(0)$.

Lemma A.4 *Suppose that the $n \times n$ matrix $P(r)$ is continuous for all $r \in [0,1]$. Suppose further that $a < b$ are two real numbers in $[0,1]$. Finally suppose that m is a positive integer, and that $h = (b-a)/m$. Then the two limits*

$$\begin{aligned} E_L(a,b;P) &= \lim_{m\to\infty} (I + h\cdot P(b))(I + h\cdot P(b-h)) \times \ldots \times \\ &\quad (I + h\cdot P(a+h))(I + h\cdot P(a)), \qquad (102) \\ E_R(a,b;P) &= \lim_{m\to\infty} (I + h\cdot P(a))(I + h\cdot P(a+h)) \times \ldots \times \\ &\quad (I + h\cdot P((b-h))(I + h\cdot P(b)) \qquad (103) \end{aligned}$$

exist. Moreover, for arbitrary real numbers $r_1,\ r_2,\ r_3 \in [0,1]$,

$$\begin{aligned} E_L(r_1,r_3;P) &= E_L(r_2,r_3;P)E_L(r_1,r_2;P), \qquad (104) \\ E_R(r_1,r_3;P) &= E_R(r_1,r_2;P)E_R(r_2,r_3;P). \qquad (105) \end{aligned}$$

Finally,

$$\begin{aligned} \frac{\partial E_L(a,b;P)}{\partial a} &= E_L(a,b;P)\cdot P(a), \qquad (106) \\ \frac{\partial E_L(a,b;P)}{\partial b} &= P(b)\cdot E_L(a,b;P), \qquad (107) \\ \frac{\partial E_R(a,b;P)}{\partial a} &= P(a)\cdot E_R(a,b;P), \qquad (108) \\ \frac{\partial E_R(a,b;P)}{\partial b} &= E_R(a,b;P)\cdot P(b). \qquad (109) \end{aligned}$$

The proof of Lemma A.4 is trivial, and is omitted here. The following lemma is an immediate consequence of the preceding one.

Lemma A.5 *Suppose that $A(r)$, $B(r)$ and $C(r)$ are three $n \times n$ matrices depending continuously on $r \in [0,1]$. Then*

$$S(r) = \int_0^r E_L(\tau, r; A)\cdot C(\tau)\cdot E_R(\tau, r; B)\cdot d\tau \tag{110}$$

is the solution of the initial value problem

$$\begin{aligned} S'(r) &= A(r)\cdot S(r) + S(r)\cdot B(r) + C(r), \qquad (111) \\ S(0) &= 0. \qquad (112) \end{aligned}$$

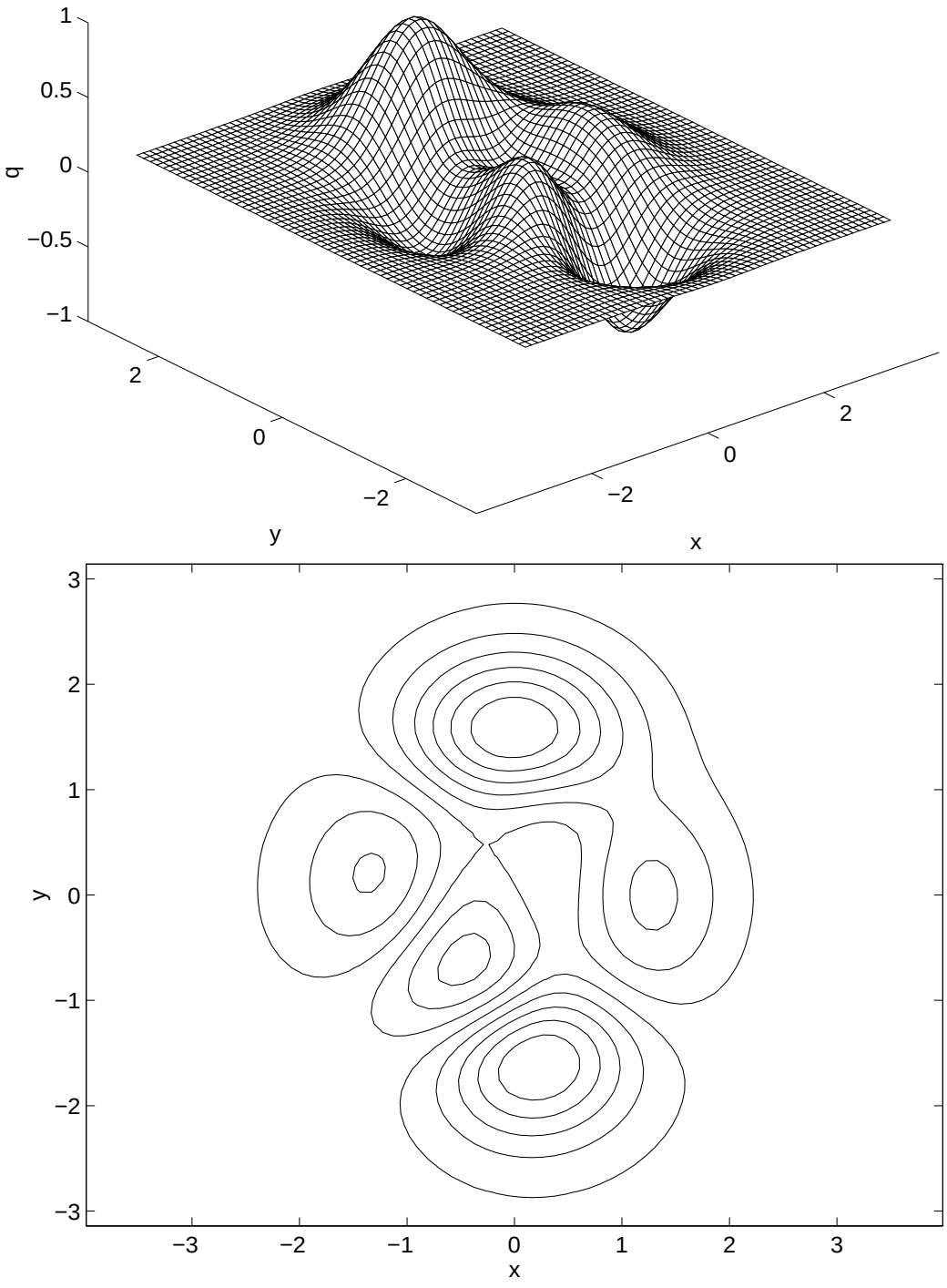

Figure 8: Surface and Contour Views of Scatterer q_1, Example 1.

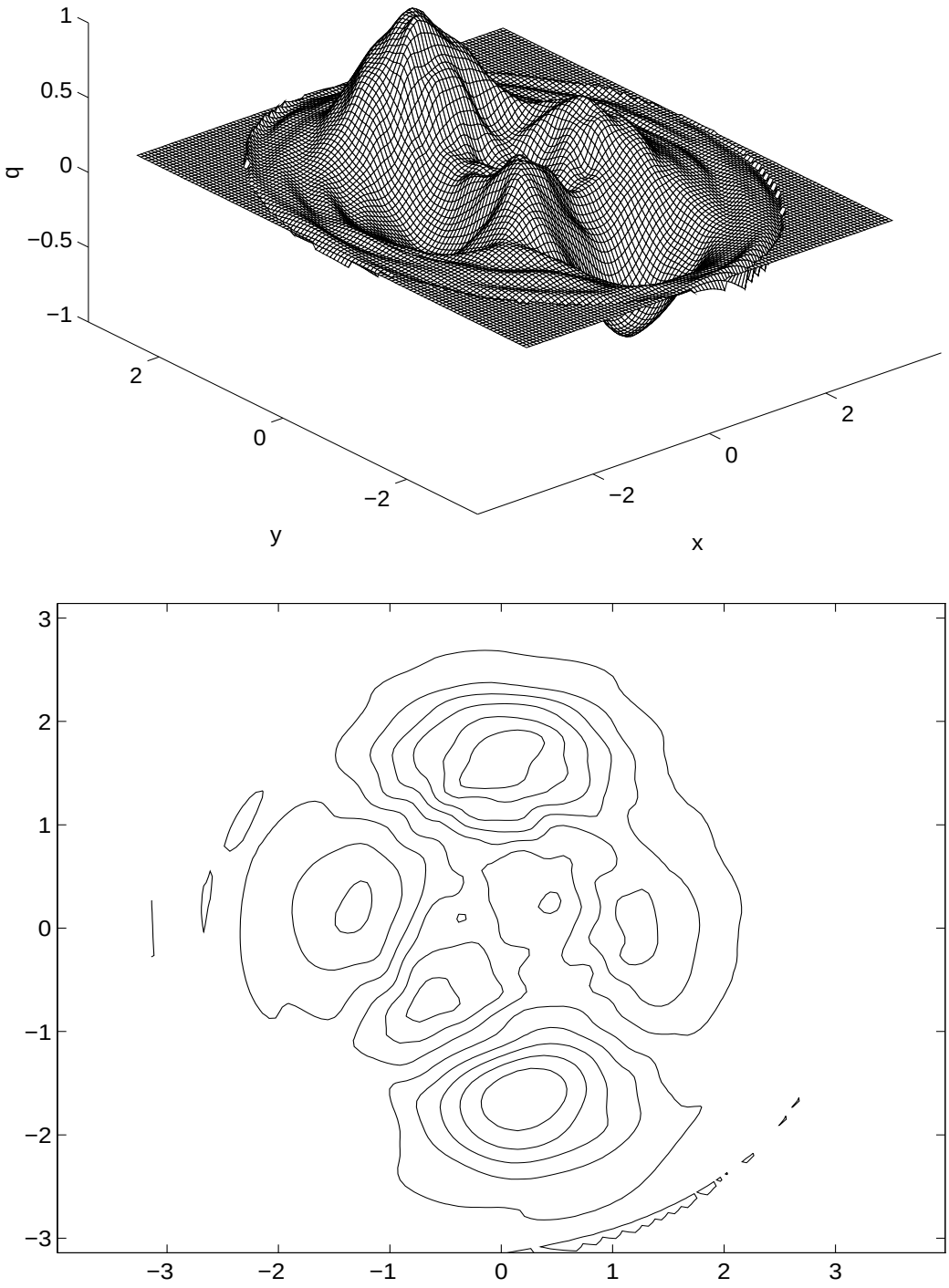

Figure 9: Surface and Contour Views of Inversion with $N_d = 1$, Example 1.1.

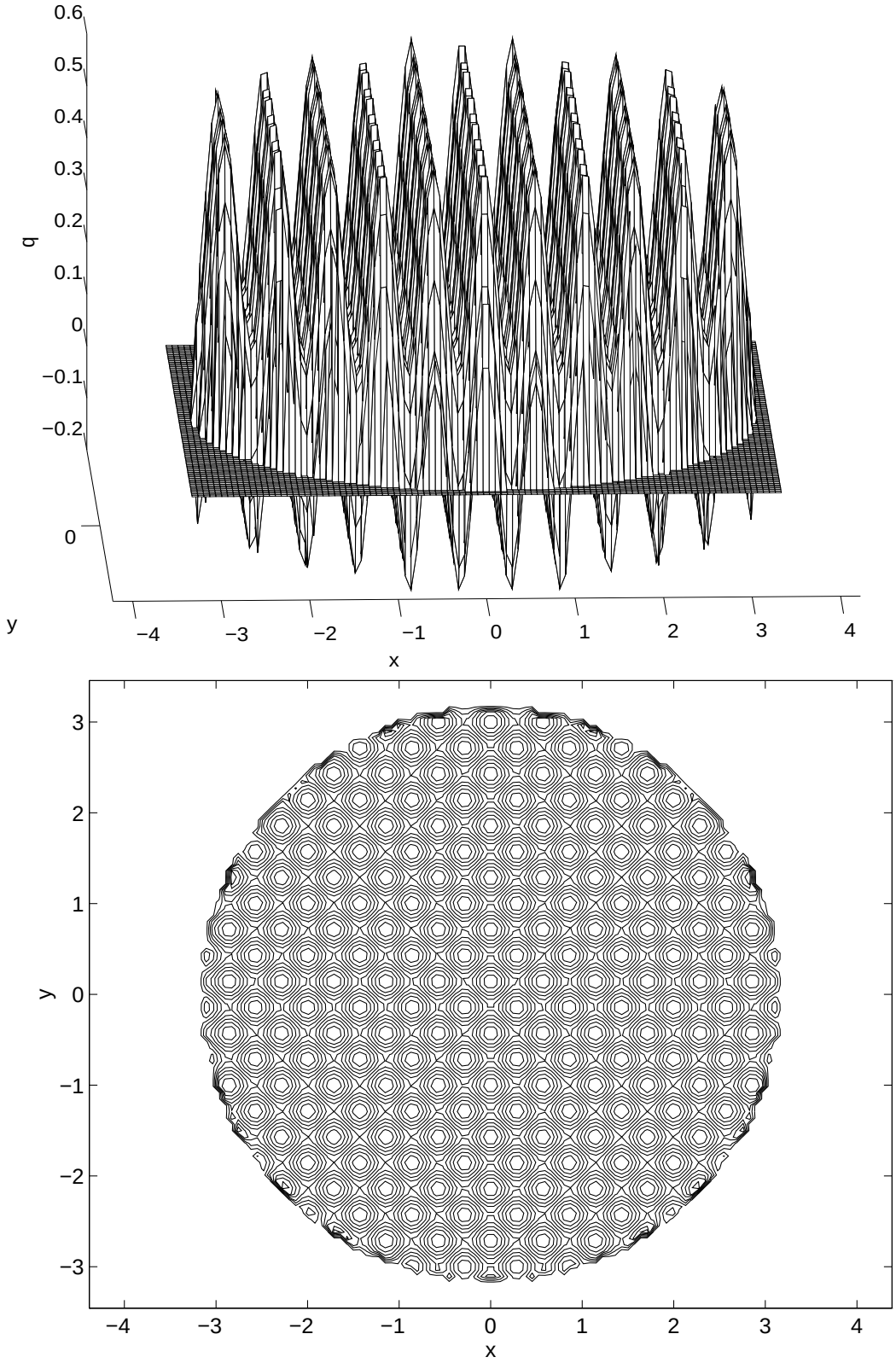

Figure 10: Surface and Contour Views of Scatterer q_2, Example 2.

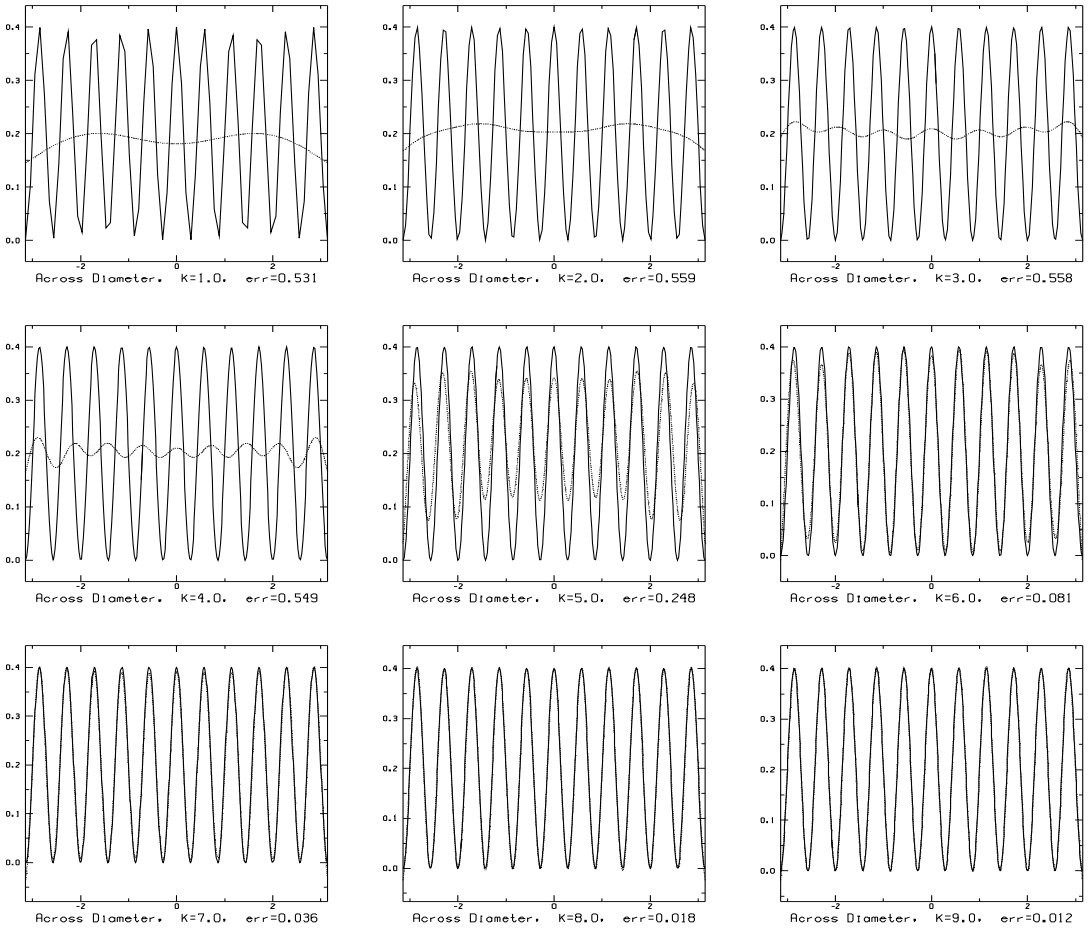

Figure 11: Reconstructed vs Exact q_2 on Diameter, $k = 1, 2, \ldots 9$, Example 2.

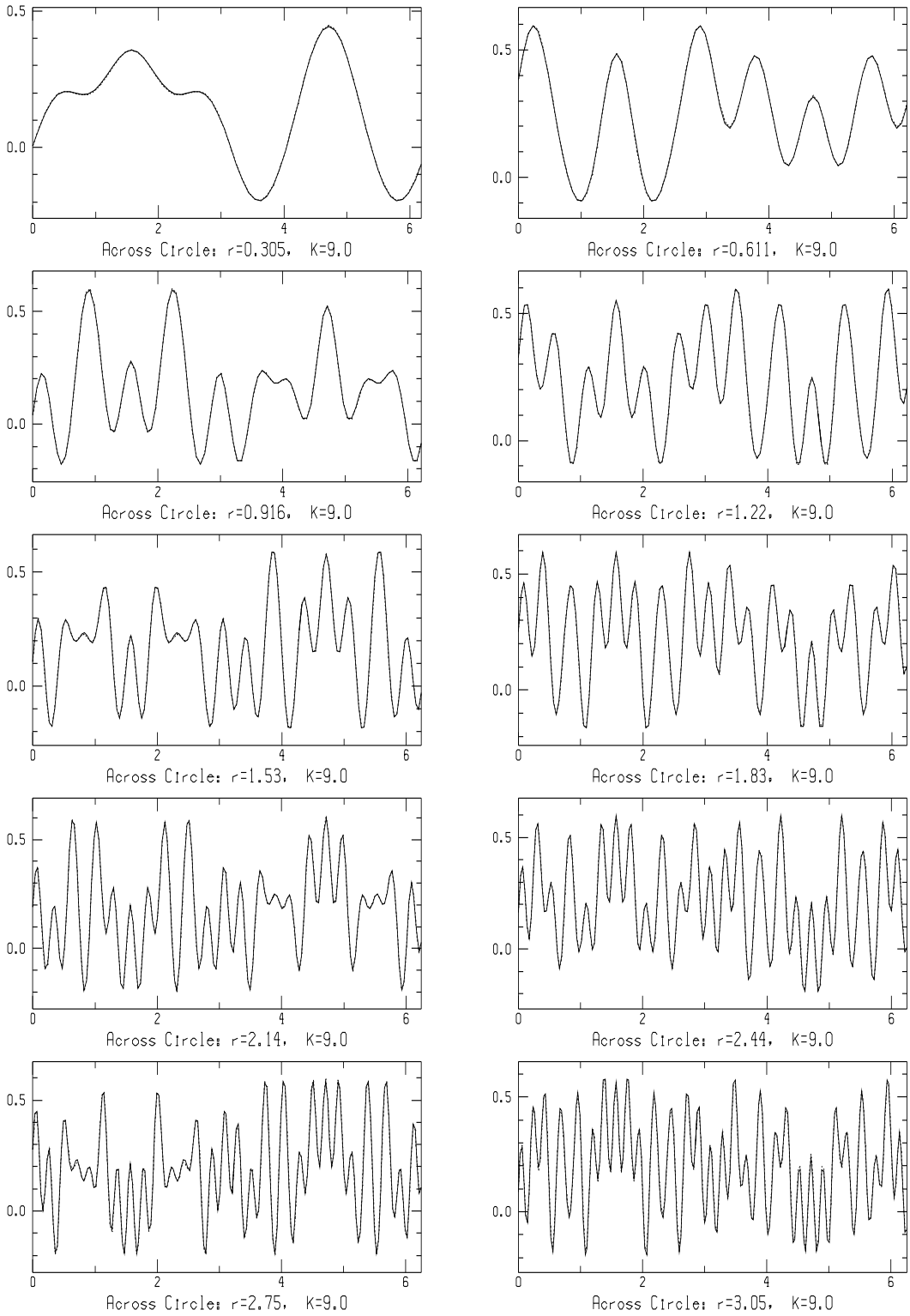

Figure 12: Reconstructed vs Exact q_2 on Circles, $k = 9$, Example 2.

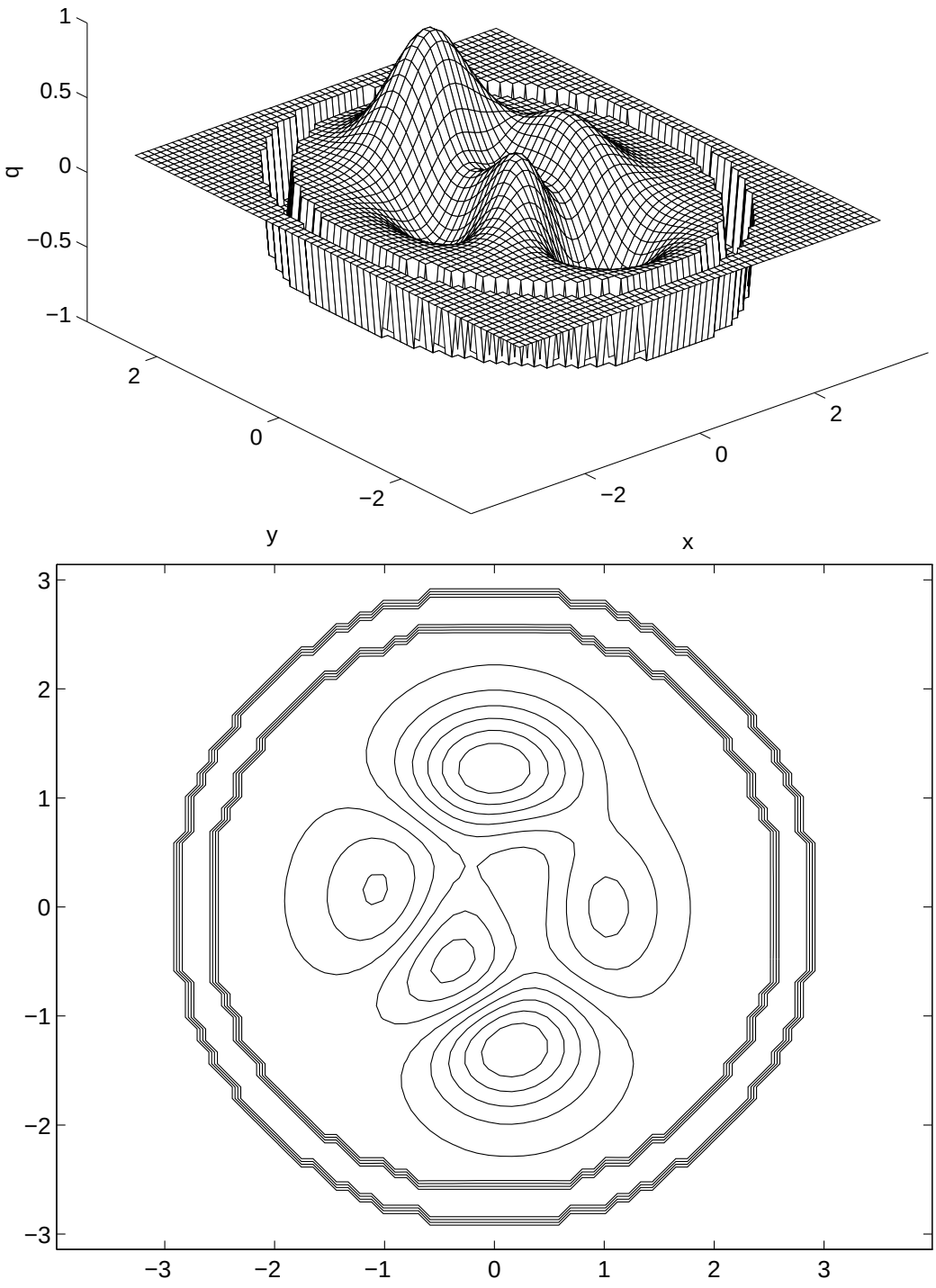

Figure 13: Surface and Contour Views of Scatterer q_3, Example 3.

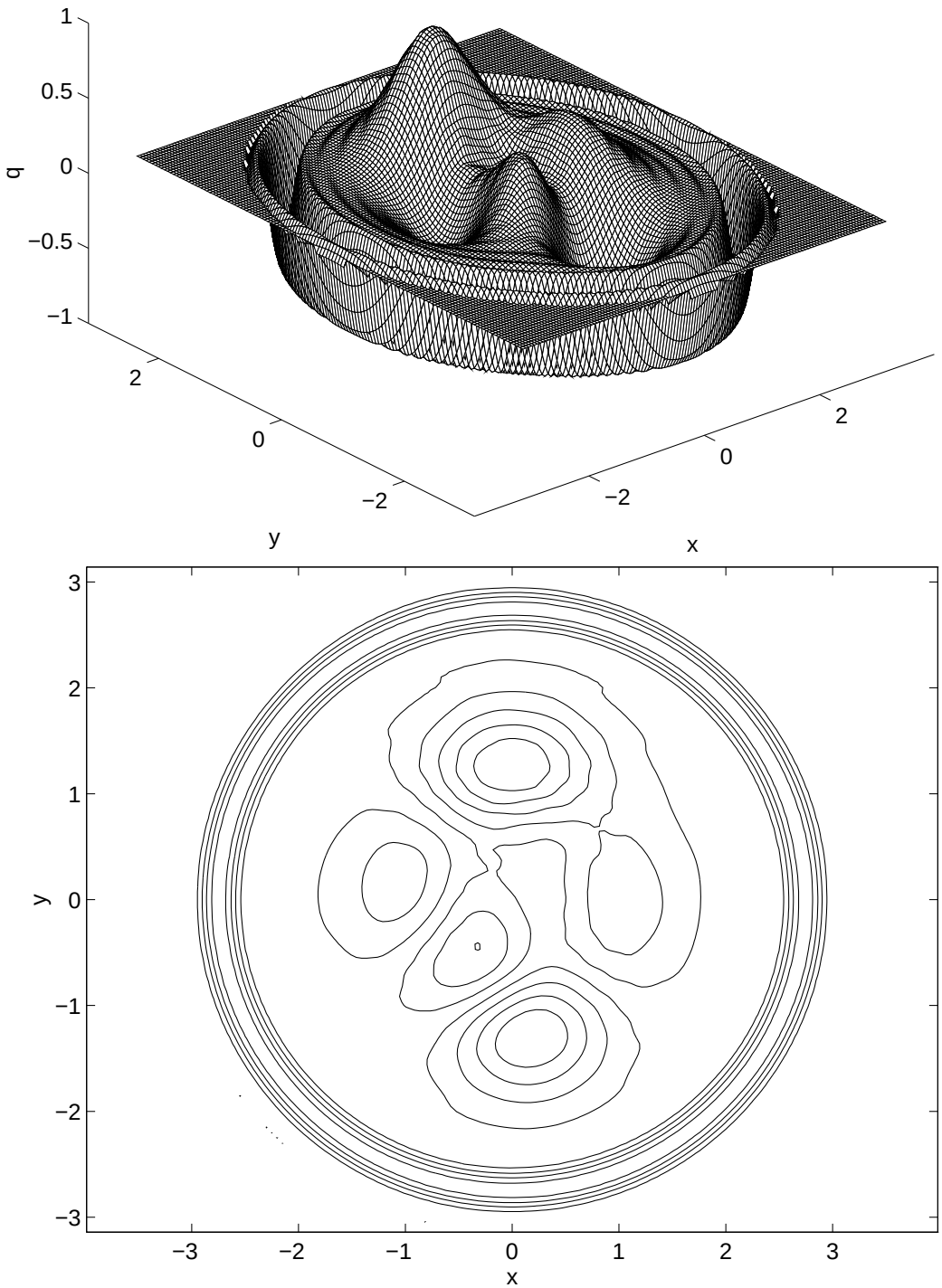

Figure 14: Surface and Contour Views of Reconstructed q_3, Example 3.

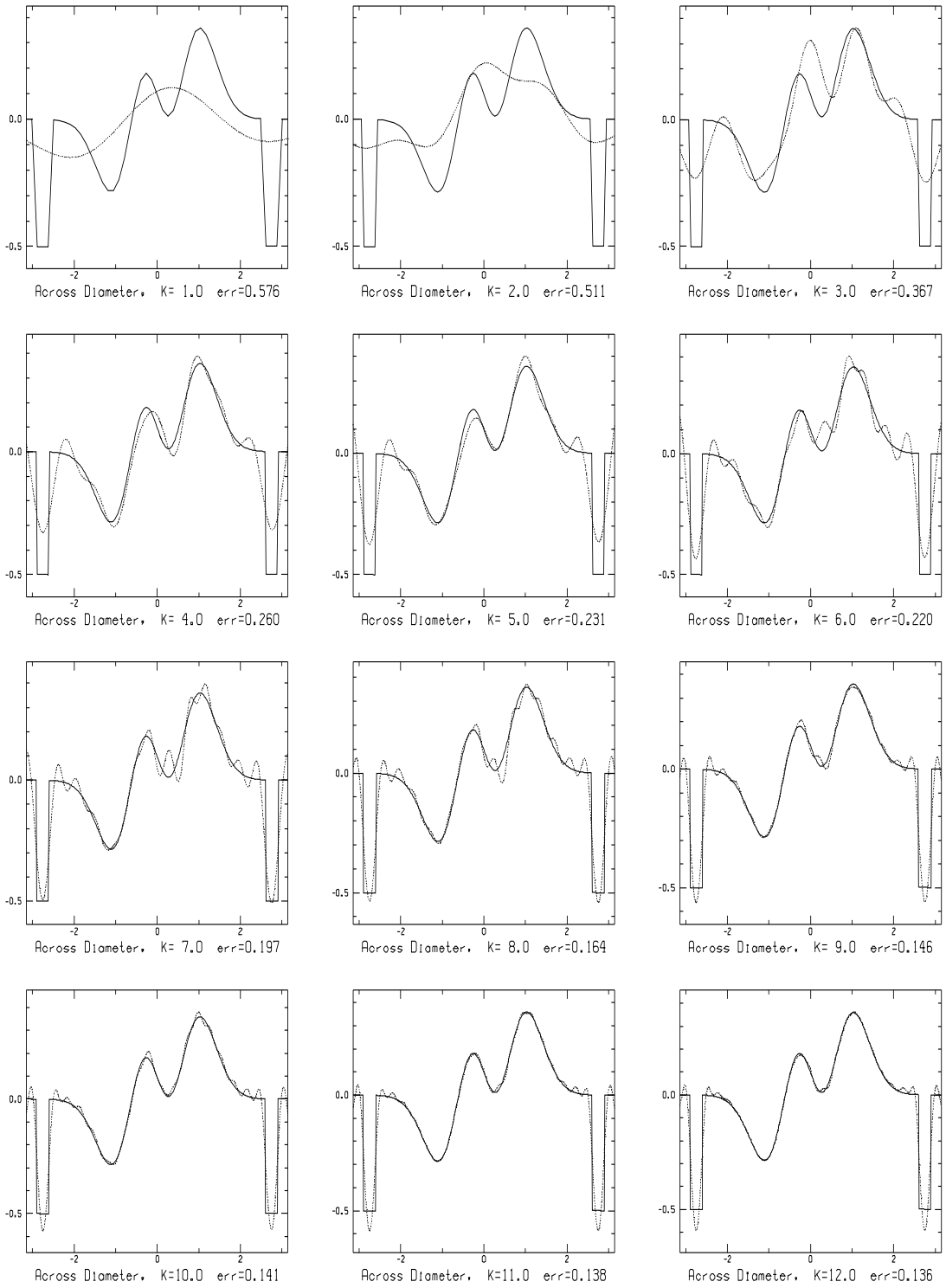

Figure 15: Reconstructed vs Exact on Diameter at 12 Frequencies, Example 3.